# MAPPING NEAR-SURFACE SALINIZATION USING LONG-WAVELENGTH AIRSAR

## SUMMARY OF RESEARCH

August 1, 1998 – July 31, 2002

by

Jeffrey G. Paine, Principal Investigator
Bureau of Economic Geology
The University of Texas at Austin

Mail address:
University Station, Box X
Austin, Texas 78713-8924\

Street address:
J.J. Pickle Research Campus, Building 130
10100 Burnet Road
Austin, Texas 78758-4445
jeff.paine@beg.utexas.edu

Report prepared for National Aeronautics and Space Administration
under NASA Grant No. NAG5-7582, SENH98-0113



August 2003

# MAPPING NEAR-SURFACE SALINIZATION USING LONG-WAVELENGTH AIRSAR

SUMMARY OF RESEARCH

August 1, 1998 – July 31, 2002

by

Jeffrey G. Paine, Principal Investigator
Bureau of Economic Geology
The University of Texas at Austin

Mail address:
University Station, Box X
Austin, Texas 78713-8924\

Street address:
J.J. Pickle Research Campus, Building 130
10100 Burnet Road
Austin, Texas 78758-4445
jeff.paine@beg.utexas.edu

Report prepared for National Aeronautics and Space Administration
under NASA Grant No. NAG5-7582, SENH98-0113



August 2003

CONTENTS



FIGURES

## TABLES

## SUMMARY

In May 1999, NASA's Jet Propulsion Laboratory acquired airborne synthetic aperture radar (AIRSAR) data over the Hatchel and Montague Test Sites in Texas. We analyzed P- and L-band polarimetric radar data from these AIRSAR missions to assess whether AIRSAR could be used as a rapid and remote platform for screening large areas at risk for near-surface soil and water salinization. Ongoing geological, geophysical, and hydrological studies at the Hatchel Test Site in Runnels County and the Montague Test Site in Montague County have demonstrated the utility of high-resolution airborne electromagnetic (EM) induction in mapping electrical conductivity changes that accompany shallow natural and oil-field related salinization at these sites in the Colorado and Red River basins.

Qualitative comparisons of single polarization and multiple-band composite radar images with co-registered apparent conductivity images show little similarity. Radar data from the Hatchel and Montague Test Sites respond strongly to vegetation attributes, land-use patterns, and infrastructure such as buildings, fences, and power lines. EM data are more closely correlated to soil properties such as mineralogy, moisture content, and pore-water chemistry.

We compared AIRSAR and airborne EM data quantitatively by (1) selecting representative flight lines from airborne EM surveys of the Hatchel and Montague sites, (2) extracting measurement locations and apparent conductivities at the highest available EM frequency, (3) identifying and extracting all P- and L-band backscatter intensities for all locations within 5 m of an airborne EM measurement, and (4) examining the spatial and magnitude relationships between apparent conductivity and all radar polarization and polarization-ratio combinations.

For both test sites, backscatter intensity in all individual P- and L-band polarizations was slightly negatively correlated with apparent conductivity. In most modes this was manifested as a decrease in the range and magnitude of backscatter intensity as apparent conductivity increased. Select single-band and cross-band polarization ratios exhibited somewhat higher correlation with apparent conductivity by partly diminishing the dominance of the vegetation contribution to

backscatter intensity. The highest correlation with conductivity was obtained using the L-band vertical- to cross-polarization ratio, the P-band vertical- to L-band cross-polarization ratio, and the P-band vertical- to cross-polarization ratio. These correlations were higher for the more arid (and less electrically conductive) Hatchel Test Site than they were for the Montague Test Site.

At its current state of development, AIRSAR data do not correlate sufficiently with airborne EM measurements of electrical conductivity to be widely useful in near-surface salinization mapping. Improvement might be achieved by increasing the incidence angle of the radar swath (making it more vertical) and recording the ground response to the transmitted radar signals for a few to a few tens of nanoseconds. Both these steps could increase the contribution of shallow soil electrical properties to the recorded backscatter signal.

# INTRODUCTION

Salinization of soil and water is a chronic concern in arid and semi-arid regions worldwide. Soil salinization reduces or eliminates crop yields and increases runoff and soil erosion; water salinization limits irrigation uses, requires expensive treatment for municipal and industrial uses, perturbs riverine ecosystems, causes fresh-water plants to be replaced by salt-tolerant ones, and affects recreational and commercial fisheries. Major potential causes of salinization include (1) natural discharge of subsurface brines; (2) upward brine movement through unplugged oil, gas, and deep water wells; (3) infiltration of produced oilfield brine beneath surface disposal pits; (4) evaporative concentration of shallow ground water as a result of irrigation or agricultural landscaping; and (5) large-scale salting of icy roadways.

In this study, which began in August 1998 and ended in July 2002, we explored whether long-wavelength (P- and L-band) AIRSAR data can be used to cost-effectively survey large areas for evidence of salinization of near-surface soil and water. Because radar reflectance can be affected by electrical properties of the ground, and because the electrical conductivity of soil and water greatly increases with salinity, we evaluated airborne radar as a screening tool to determine areas where higher resolution airborne geophysical surveys and soil and water sampling are warranted. We explored the usefulness of AIRSAR at two test sites where high-resolution airborne surveys, extensive ground-based geophysical measurements, and soil and water sampling have been completed. We expect radar reflectance to be influenced by ground conductivity (particularly at the longer P- and L-band wavelengths) and expect some degree of correlation between radar reflectance images at these wavelengths with ground conductivity images at the highest EM frequencies recorded during our ongoing studies of these test areas. The work is (1) a response to the realization that it is too expensive to collect helicopter-based, low-altitude, high-resolution conductivity data over large regions where near-surface salinization is a threat to agriculture, fisheries, and drinking-water supplies, and (2) the next step in an ongoing effort to

develop an integrated methodology that can identify near-surface salinization using a combination of remote sensing imagery, airborne EM measurements, and limited soil and water sampling.

For this project, NASA collected and processed AIRSAR data in two test areas (fig. 1): (1) within the Colorado River basin near San Angelo in West Texas (Hatchel Test Site), where a 1996 high-resolution airborne EM survey revealed the presence of natural, oilfield-related, and agricultural salinity sources, and (2) within the Red River basin of Texas and Oklahoma (Montague Test Site), where a 1997 airborne geophysical study of salt-impacted agricultural lands revealed oilfield-related salinization extending over many square kilometers. This technical report summarizes our research activities during this project.

## Hatchel Test Site

The Hatchel study area occupies a 91-km$^2$ area within the Hatchel quadrangle in Runnels County, Texas (figs. 1 and 2). This area is on the eastern flank of the Southern Great Plains, which slopes gently southeastward from eastern New Mexico to central Texas, and at the southern end of the Rolling Plains. Physiographic features of the Hatchel area include gently rolling, dissected uplands and valleys formed by the southward-draining Elm and Coyote Creeks and their tributaries. Surface elevations range from as high as 525 m on the dissected uplands to 460 m within the Elm and Coyote Creek drainages (fig. 3). Climate is semiarid; average annual precipitation is 52 cm at San Angelo (Bomar, 1983), located about 60 km southwest of the study area.

Rock and soil type can influence ground conductivity, but the effect of the host material on ground conductivity is generally much less than that caused by moisture content and ionic concentration in pore fluids. Clayey soils and rocks are generally more conductive than sandy units (McNeill, 1980; Rhoades, 1981). Geologic units (Kier and others, 1976) at the surface or in the shallow subsurface include (a) Quaternary alluvium that is generally sandy, has relatively high water content, and is found in topographic lows along streams, (b) thin Pleistocene terrace

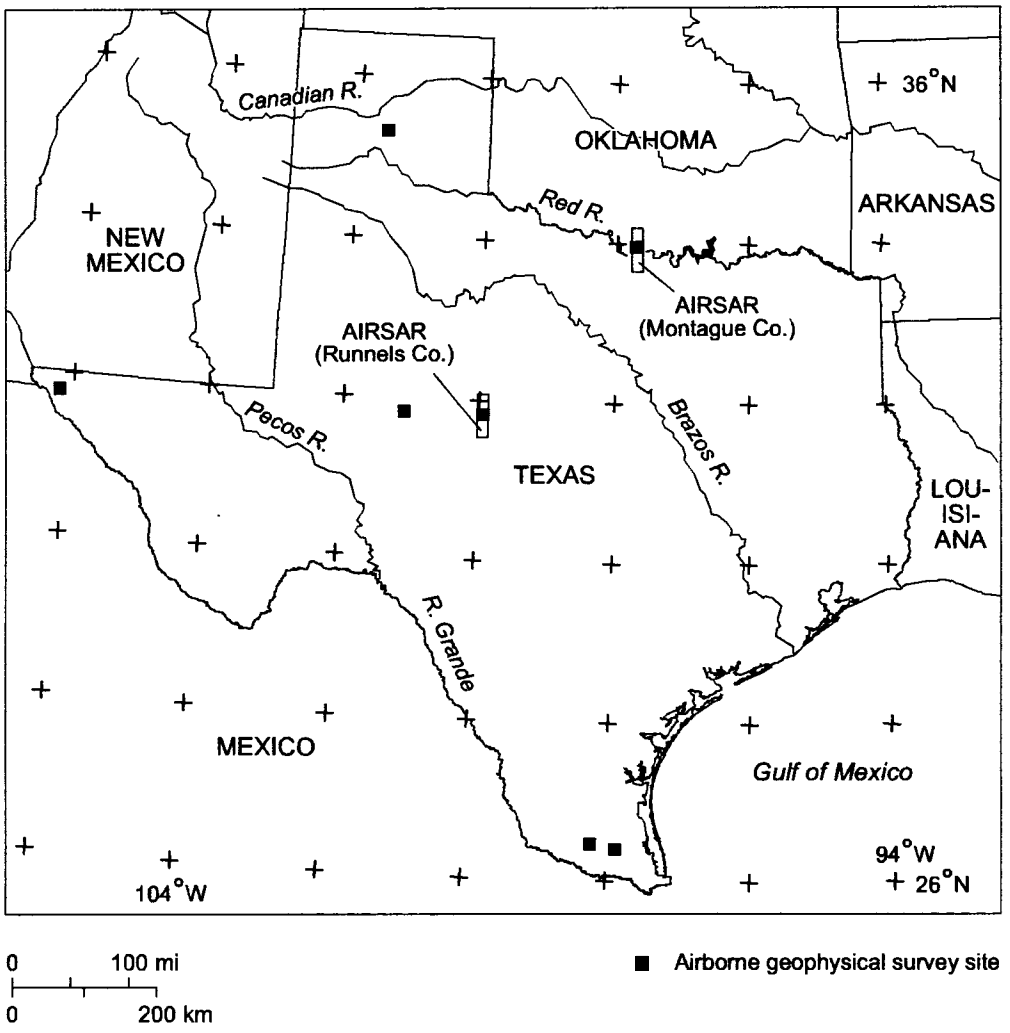


Figure 1. Regional map showing the locations of recent (1996 to 2003) airborne geophysical surveys in Texas (solid squares) and the boundaries of the 1999 AIRSAR surveys in Runnels and Montague Counties, Texas (open rectangles).

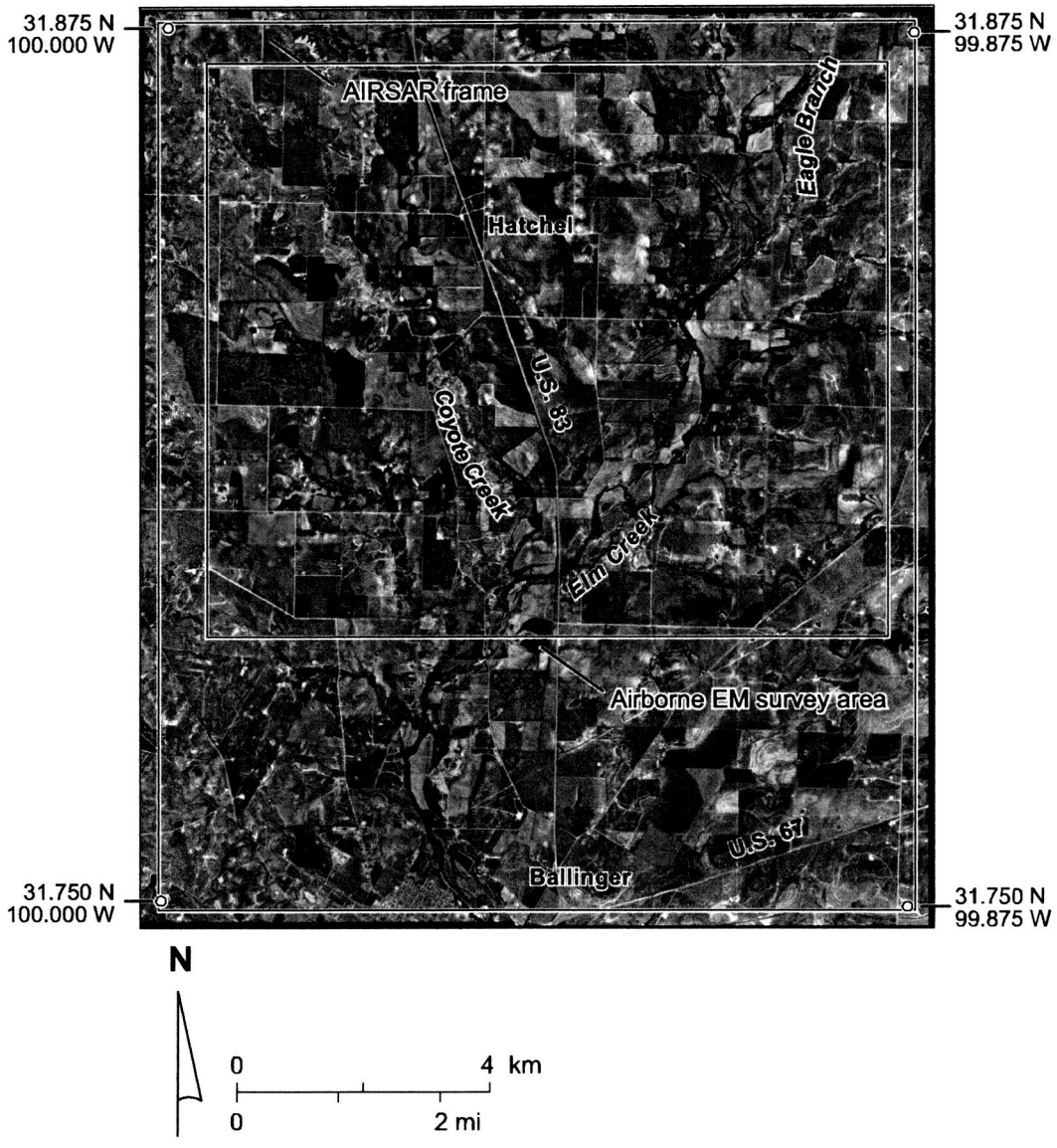


Figure 2. Digital orthophotomosaic of the Hatchel quadrangle, Runnels County, Texas. Also shown are the boundaries airborne electromagnetic induction survey of the Hatchel Test Site and the AIRSAR data used for comparison with the EM data.

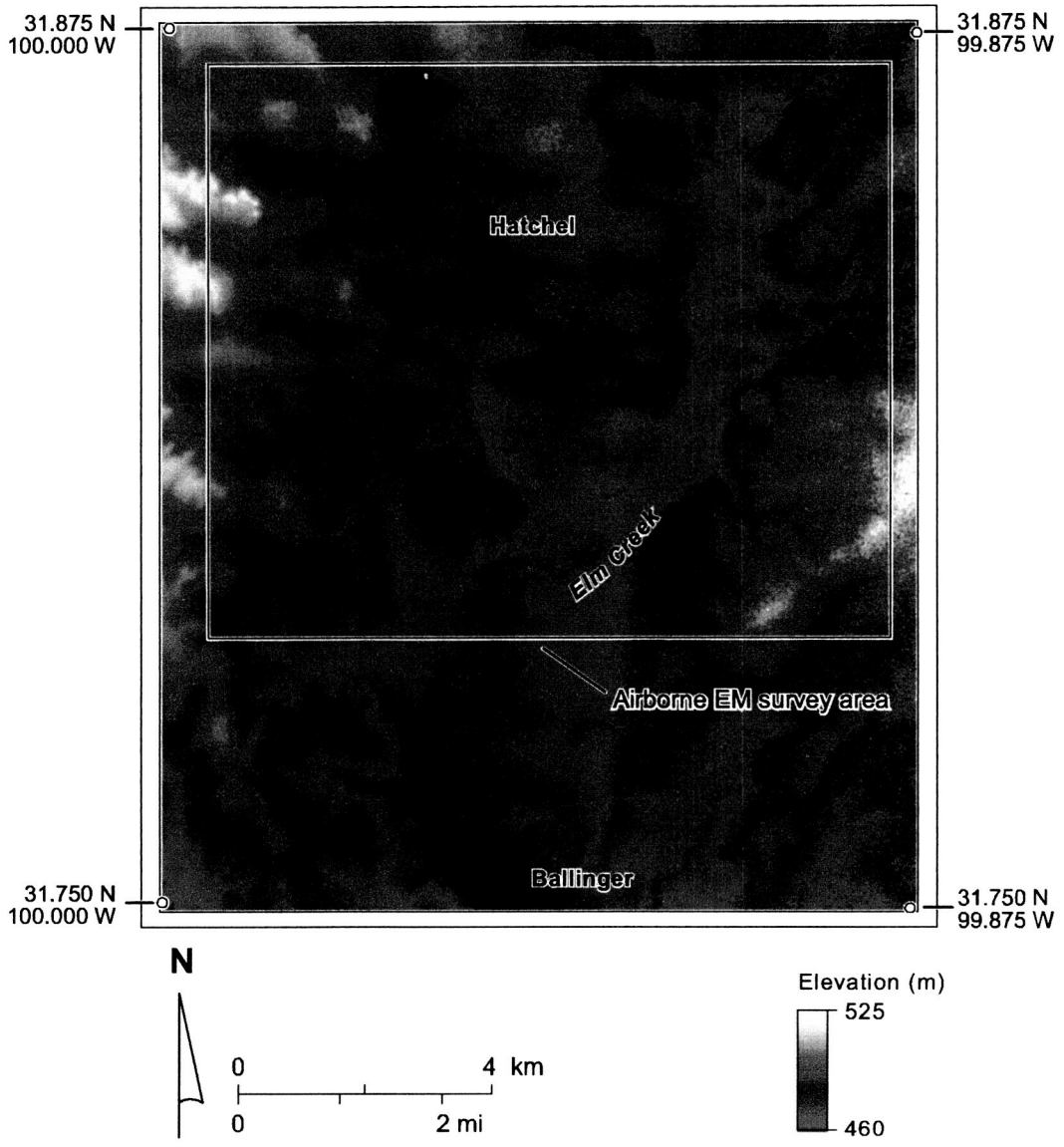


Figure 3. Digital elevation map of the Hatchel quadrangle, Runnels County, Texas, derived from C-band AIRSAR interferometry. East-west banding is a processing artifact.

deposits that are composed of clay to gravel, are relatively dry, and are mapped at higher elevations along the central part of the study area, and (c) outcrops of Permian Clear Fork Group strata and the Lueders Formation containing units of sandstone, limestone, shale, and marl. Permian stratigraphic units dip west-northwestward into the Permian Basin.

Soil type can affect measured ground conductivities for high-frequency, shallow-penetrating conductivity instruments. Soils have been mapped in greater detail than have the geologic units for the study area (Wiedenfeld and others, 1970). On the lowlands, deep, loamy, relatively wet soils of the Spur-Colorado-Miles association are formed on Quaternary alluvium. These soils generally contain less clay than the upland soils, but may have higher conductivity because they are thicker, wetter, and in many places contain conductive pore water. Soils on the uplands are generally the shallow, clayey to loamy, and relatively dry residual soils of the Portales-Potter-Mereta association that form on the Pleistocene terrace deposits and Permian Clear Fork Group strata. Despite their relatively high clay content, these soils have low measured conductivity due to their thinness and low moisture content.

## Montague Test Site

The Montague study area encompasses 35 $km^2$ along the Red River in Montague County, Texas (figs. 1 and 4). It is located within the Prairie Valley School quadrangle on the southern flank of the Red River valley. This semiarid area averages about 100 cm precipitation annually (Bomar, 1983).

Topography is dominated by the Red River, its eroded valley, and its modern deposits and older terraces (figs. 4 and 5). Major physiographic features in the quadrangle include (a) the dissected Permian upland at elevations of about 210 to 260 m that covers the southern half and northwestern corner of the quadrangle; (b) the Red River and its modern deposits at the lowest elevations of 180 to about 200 m; and (c) an older Red River alluvial terrace at elevations of 200 to 210 m on the southern flank of the river (figs. 4 and 5). Outcropping geologic units include

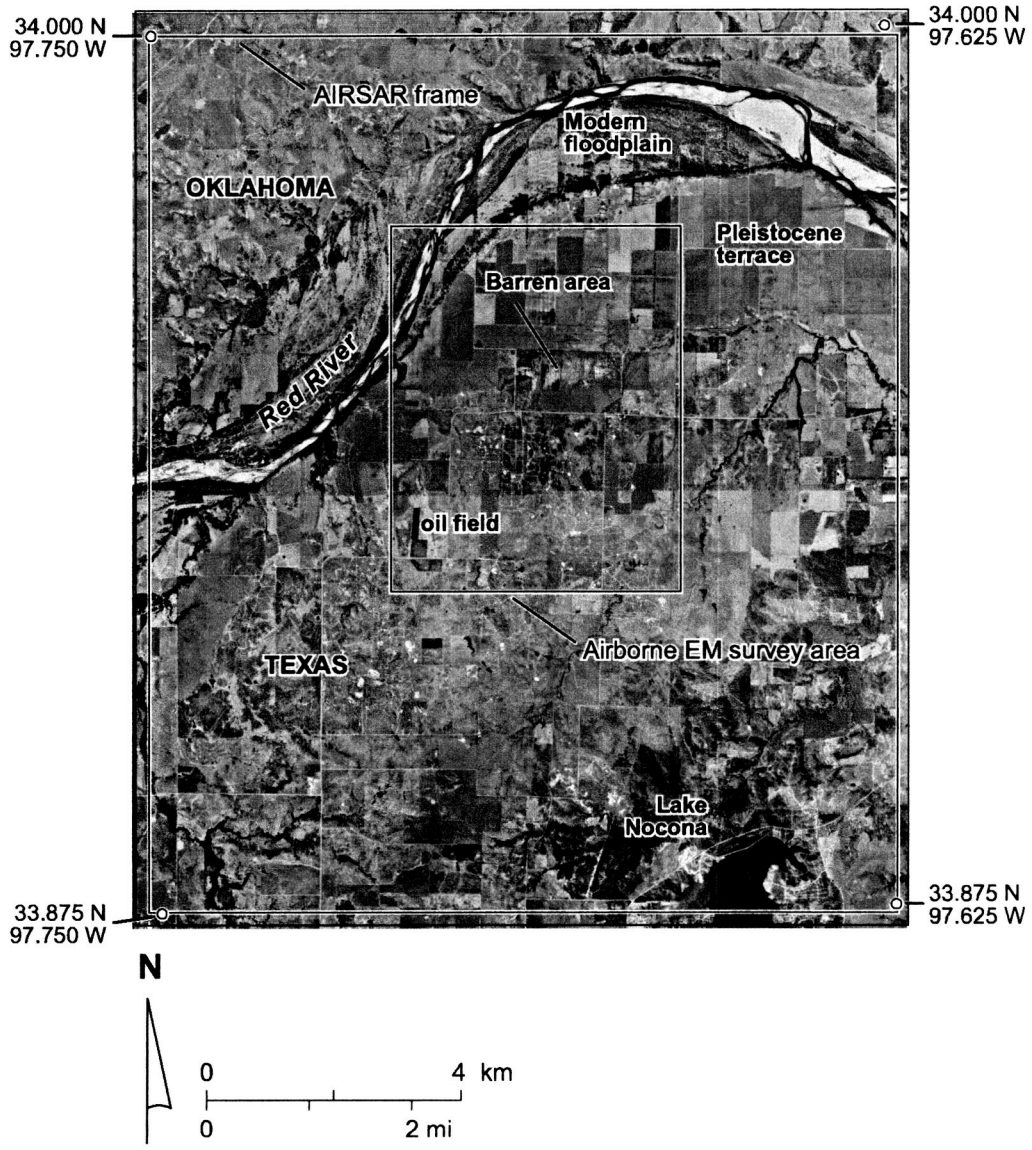


Figure 4. Digital orthophotomosaic of the Prairie Valley School quadrangle, Montague County, Texas. Also shown are the boundaries airborne electromagnetic induction survey of the Montague Test Site and the AIRSAR data used for comparison with the EM data.

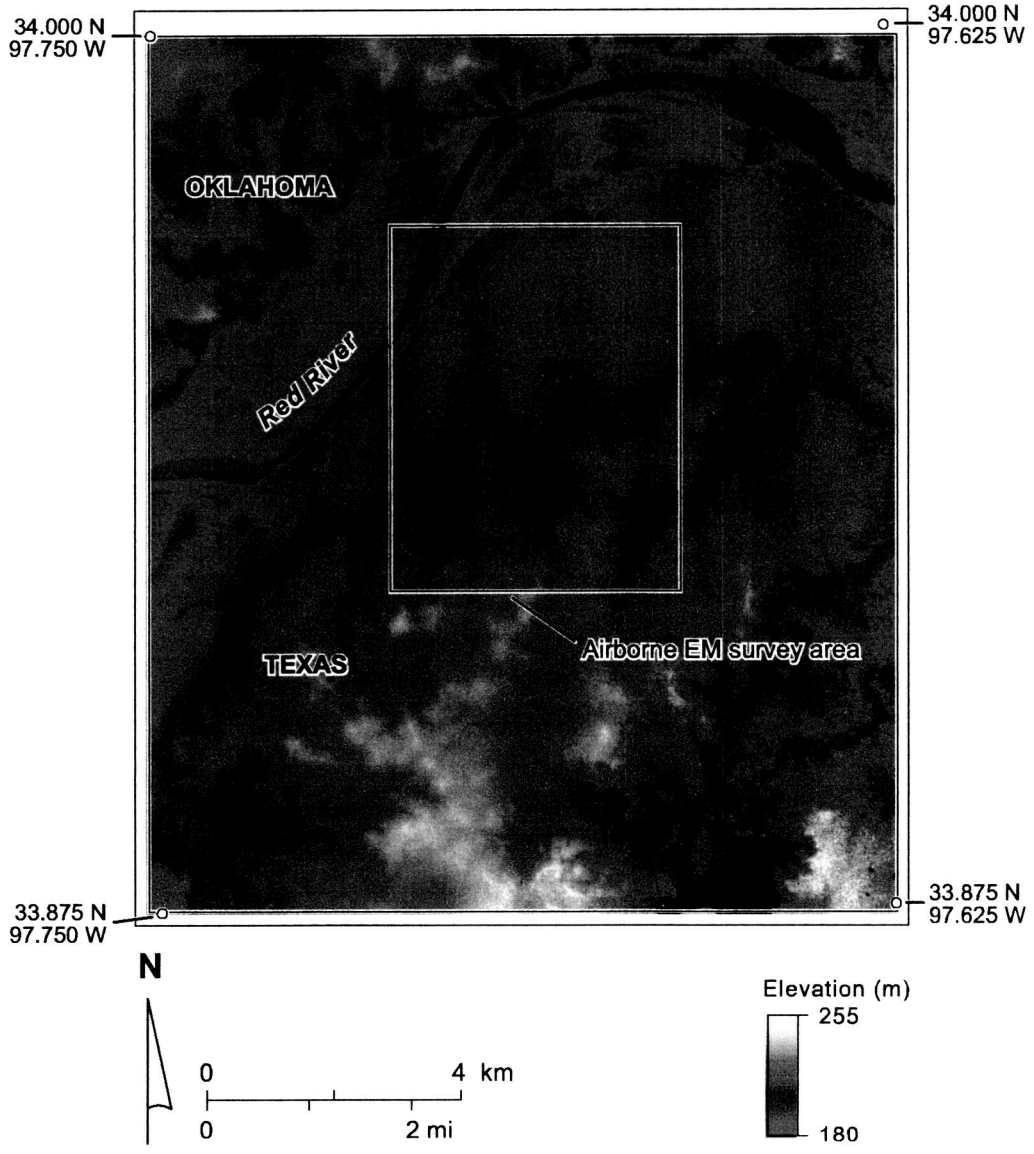


Figure 5. Digital elevation map of the Prairie Valley School quadrangle, Montague County, Texas, derived from C-band AIRSAR interferometry. North-south banding is a processing artifact.

fluvial sandstones and mudstones of the Permian Nocona Formation (McGowen and others, 1991; Hentz, 1988) and a series of Tertiary and Quaternary alluvial and eolian sediments (Frye and Leonard, 1963). Permian sandstones are exposed on upland areas, hill crests, road cuts, and in stream banks, particularly in the southern part of the quadrangle. Farther north and closer to the Red River, Permian units are blanketed by as much as several meters of more recent wind-blown and river-borne sediments.

The post-Permian deposits consist of unlithified gravel, sand, silt, and clay deposited by the ancestral Red River and its tributaries, or silt and sand blown across the valley and deposited on river terraces and Permian outcrops. At least three episodes of Red River alluvial activity are represented in the quadrangle, including sandy modern channel and muddy floodplain deposits in the modern terrace, an extensive and well-preserved older, intermediate terrace that is as much as 3 km wide and more than 15 m higher than the modern floodplain, and gravel lag and finer grained alluvial deposits that are exposed at higher elevations and generally thicken toward the river valley. Inset into these older alluvial deposits on the upland are much younger and less extensive alluvial sediments transported by small streams that drain the upland.

Eolian silts and sands are found as vegetated and stabilized dunes where the modern and intermediate terraces meet and as blanket deposits overlying older terrace alluvium on the uplands. Like the alluvial deposits, the age of the windblown deposits generally increases southward from the river.

Extensive oil and gas discoveries in what eventually became the Nocona North and Spanish Fort oil fields began in the 1920s (McBee and Vaughan, 1956), some four decades before salt-water discharge related to oilfield production was regulated in Texas. Consequently, millions of barrels of co-produced salt water have been discharged onto the ground and into pits and creeks. Near-surface salinization of soil and water has killed vegetation, contaminated shallow water wells, enhanced surface erosion, and increased the salinity of the Red River (Hovorka and others, 1999). Most sources of salinity are located in the oil fields on Permian bedrock; the most significant impacts of salinization occur on cultivated alluvial terrace deposits of the Red River. Barren

areas have formed where salt water has been discharged at the surface and where salt water has reached the surface through ground-water flow or overland transport.

## METHODS

The principal methods employed in this study are airborne electromagnetic induction (EM) and airborne synthetic aperture radar (AIRSAR). We have used airborne EM in several recent studies of shallow soil and water salinization and have found it to effectively map salinization through the increase in ground conductivity that accompanies salinization. Because radar is also an electromagnetic phenomenon and can be used to rapidly map large areas at reasonably high resolution, we wished to compare the EM and radar response over two areas where the extent and intensity of salinization is well known.

### Airborne Electromagnetic Induction

Electromagnetic induction (EM) methods (Parasnis, 1973; Frischknecht and others, 1991; West and Macnae, 1991) were used to measure apparent electrical conductivity of the ground at the Runnels and Montague Test Sites using airborne (fig. 6) and ground-based instruments. EM methods employ a changing primary magnetic field created around a transmitter coil to induce a current to flow in the ground, which in turn creates a secondary magnetic field that is sensed by the receiver coil. In general, the strength of the secondary field is proportional to the conductivity of the ground. An assumption is that the near-surface environment consists of horizontal layers of infinite lateral extent. This is not strictly true anywhere, but near-surface layers have sufficient lateral extent in both study areas to validate the assumption.

Exploration (skin) depth, defined as the depth at which the primary field strength is reduced to 1/e times its original value, depends on both the conductivity of the ground and the frequency of the instrument. Skin depth is calculated using the equation

$$d = k\,(\rho / f)^{0.5}$$

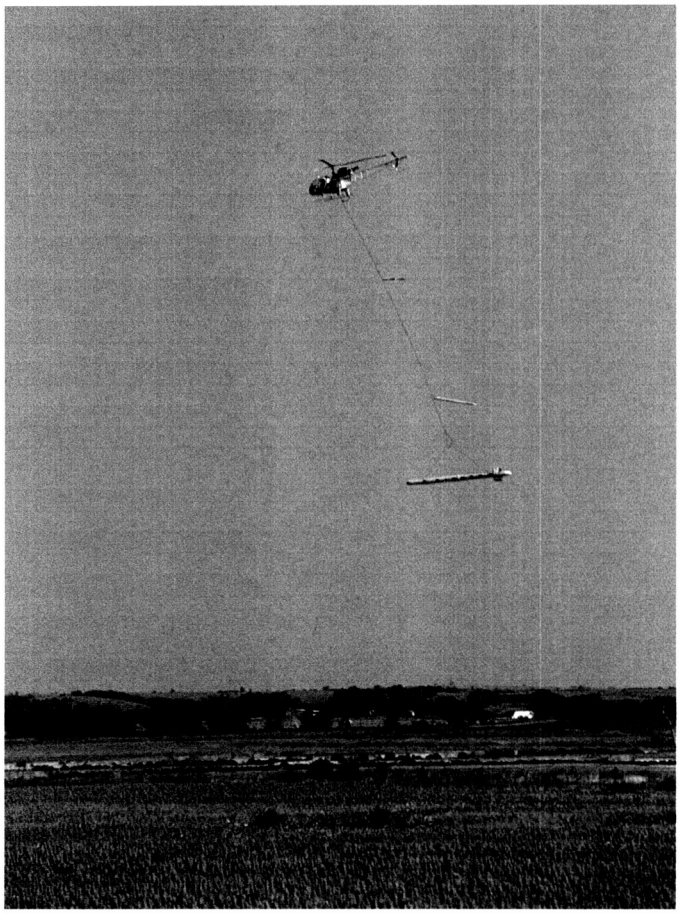

Figure 6. The DIGHEM$^{V}$ airborne EM system at the Montague Test Site. The lower bird contains five pairs of induction coils and is used to measure the apparent electrical conductivity of the ground. The upper bird is the Cesium magnetometer used to measure magnetic field strength.

where d = skin depth (in m), k = 500 $(m/ohm\text{-}s)^{0.5}$, $\rho$ = resistivity (in ohm-m), and f = EM frequency (in cycles/s) (Telford and others, 1976). Recast into equivalent, reciprocal conductivity terms, this equation becomes

$$d = k\,(1 / \sigma f)^{0.5}$$

where k = 15,681 $(m\text{-}mS/s)^{0.5}$, $\sigma$ = conductivity (in mS/m), and f = EM frequency.

Exploration depths for the 56,000-Hz coils, calculated from the known frequency and from the observed apparent conductivity range of 25 to 3,000 mS/m, increase from about 1 m for the most conductive ground to about 14 m for the least conductive ground (fig. 7). Apparent conductivities measured by the 7,200-Hz coils, ranging from 25 to 1,500 mS/m in the study areas, are lower than those measured by the 56,000-Hz coils. Exploration depths for this frequency are between 5 and 38 m, decreasing with increasing conductivity. At 900 Hz, airborne coils measured apparent conductivities that ranged from 25 to 500 mS/m. Exploration depths for this frequency are between 25 m for the most conductive ground to more than 75 m for the least conductive ground. We chose the highest frequency (shallowest exploration depth) for quantitative comparisons with AIRSAR data. This frequency senses deeply enough to identify salinized soil and groundwater, yet as the shallowest sensing frequency has the greatest likelihood of correlation with shallowly penetrating radar waves of the frequencies acquired with the AIRSAR system.

## Hatchel Airborne EM Survey

Dighem, a minerals exploration company based in Canada, surveyed the Hatchel study area in Runnels County, Texas with helicopter-based geophysical instruments in January 1996 (Garrie, 1996). Principal instruments mounted in the helicopter were the DIGHEM$^{V}$ system that measures ground conductivity using five EM coil pairs and measures magnetic field strength using a Cesium vapor magnetometer. The EM coils and the magnetometer were slung beneath the helicopter (fig. 6) at nominal heights of 30 m for the coils and 40 m for the magnetometer (table 1). The helicopter maintained a height of 60 m and flew at an average speed of 108 km/hr (Garrie,

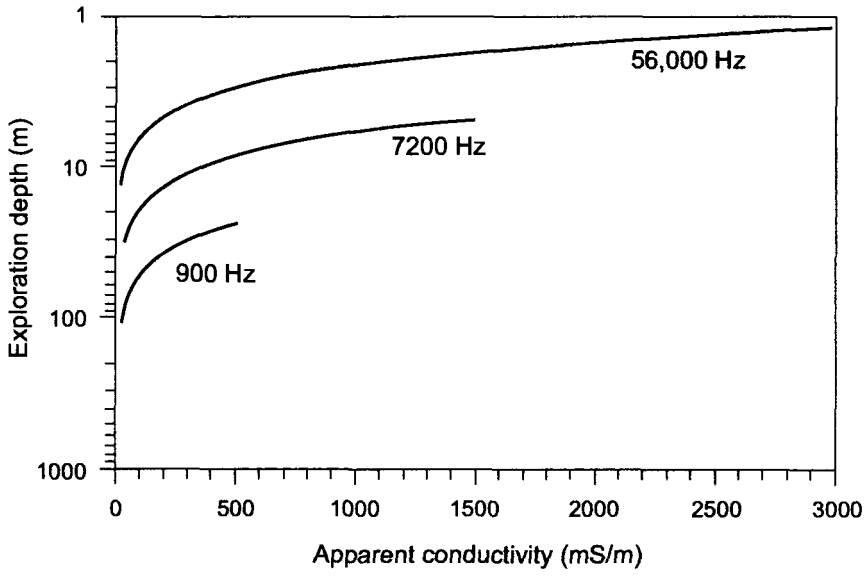


Figure 7. Estimated exploration depth (skin depth) for induction coils operating at 900, 7,200, and 56,000 Hz over a horizontal half space with apparent conductivities within the range of those measured in the Hatchel and Montague airborne EM surveys.

Table 1. Survey and flight parameters for the airborne electromagnetic induction surveys in Montague and Runnels Counties, Texas.

| | **Montague Test Site** | **Hatchel Test Site** |
|---|---|---|
| Location | Montague County, Texas | Runnels County, Texas |
| Acquisition date | July 25, 1997 | January 14-17, 1996 |
| Helicopter | Aerospatiale SA315B | Lama 315 |
| Flight speed (m/s) | 33 | 30 |
| Line spacing (m) | 100 | 100 |
| Sample spacing (m) | 3 | 3 |
| Aircraft height (m) | 60 | 60 |
| EM system | DIGHEM$^{V}$ | DIGHEM$^{V}$ |
| Instrument height (m) | 30 | 30 |
| Coil frequencies (Hz) | 900, 7,200, 56,000 | 900, 7,200, 56,000 |
| Area surveyed (km$^2$) | 27 | 91 |
| Samples | 38,936 | 157,187 |

1996). Supporting instruments included a differential GPS navigation system with locational accuracy to 5 m and a radar altimeter.

Flight lines for this high-resolution survey were oriented east-west, were spaced 100 m apart, and covered a total length of 940 km within the 91 $km^2$ Hatchel area (fig. 2). EM and magnetometer data were sampled at 0.1 s intervals, corresponding to a sample spacing of about 3 m along each flight line. EM coil separations of 6 to 8 m and a bird height of 30 m suggest a footprint a few tens of meters wide. EM and magnetometer data were processed by Dighem (Garrie, 1996). Images of ground conductivity at three coil frequencies (900, 7,200, and 56,000 Hz in a vertical dipole orientation) and total and enhanced magnetic field strength were imported into a geographic information system for spatial analysis.

Montague Airborne EM Survey

Boundaries and acquisition parameters were chosen for the airborne EM survey of the Montague site based on results of reconnaissance, ground-based measurements made using a Geonics EM34-3 ground conductivity meter. Airborne, frequency-domain EM data were acquired in January 1997 by Geoterrex-Dighem using helicopter-borne horizontal coplanar coils operating at 900, 7,200, and 56,000 Hz and vertical coaxial coils operating at 900 and 5,500 Hz at an instrument height of 30 m and a flight-line spacing of 100 m over the 35-$km^2$ study area (fig. 4 and table 1). Geoterrex-Dighem processed the airborne data, calculating apparent halfspace conductivities for each coplanar coil frequency at each measurement point (Garrie, 1997). Measurement spacing along each flight line was 3 m, providing the high-resolution coverage needed to identify salinity sources and quantify salinized areas accurately. Similar airborne surveys have been completed in Mississippi (Smith and others, 1997) and West Texas (Paine and others, 1997; Paine and others, 1999) to locate conductivity and magnetic-field anomalies associated with oil-field salinity sources that include brine-disposal pits, surface spills, and leaking wells.

## Airborne Synthetic Aperture Radar (AIRSAR)

NASA's Jet Propulsion Laboratory (NASA/JPL) operates the AIRSAR system from a modified DC-8 aircraft. Polarimetric and interferometric radar data are acquired at three frequencies (C, L, and P band) that have characteristic wavelengths (table 2) of about 6 cm (C band), 24 cm (L band), and 68 cm (P band). In contrast to airborne EM systems, which operate on slow- and low-flying aircraft over relatively small areas, the AIRSAR system is flown at high speed and high altitude (about 8 km), allowing rapid coverage of relatively large areas.

Radar scattering is governed by wavelength, incidence angle, target size, and target electrical properties. At the high frequencies and relatively short wavelengths employed by the AIRSAR system, relatively little radar penetration into the subsurface is anticipated. Nevertheless, because AIRSAR is a multi-frequency system, electrical properties of the soil can influence the scattering behavior of longer wavelengths proportionately more than shorter wavelengths. This difference in scattering response potentially provides a means of detecting areas of increased soil conductivity associated with salinization by comparing scattering response at both L and P wavelengths.

On May 21, 1999, NASA/JPL acquired AIRSAR data over one 7.5-minute quadrangle in Runnels County, Texas (Hatchel quadrangle) and one quadrangle in Montague County, Texas (Prairie Valley School quadrangle) (figs. 2 and 4). TOPSAR data included northbound and southbound flight lines 60 km long over each area using the XTI1P mode at 20 MHz (table 3). This TOPSAR mode provides L- and P-band polarimetry (horizontal polarization [HH], vertical polarization [VV], and cross polarization (HV), and C-band interferometry and VV polarization. Additionally, NASA/JPL acquired L-band polarimetric data at 80 MHz over the Runnels site. We selected and prioritized six 25-km-long data segments for processing, including parts of the north- and south-oriented TOPSAR lines for both test sites and the north-oriented 80-MHz POLSAR line for the Runnels site. NASA/JPL delivered processed data for the north- and south-

Table 2. AIRSAR bands, frequencies, wavelengths, and polarizations used in the Montague and Runnels surveys.

| Band | Frequency (GHz) | Wavelength (cm) | Polarizations |
|---|---|---|---|
| C | 5.4 | 5.6 | VV |
| L | 1.25 | 24 | HH, HV, VV |
| P | 0.44 | 68 | HH, HV, VV |

Table 3. AIRSAR flight lines, dates, acquisition modes, and flight parameters.

| Flight line | Product ID | Flight Date | Mode | Heading | Length (km) |
|---|---|---|---|---|---|
| Montague 360-1 | TS1014 | 5/21/1999 | XTI1p, 20 Mhz | 0 | 60 |
| Montague 180-1 | TS1016 | 5/21/1999 | XTI1p, 20 MHz | 180 | 60 |
| Runnels 360-1 | CM5641 | 5/21/1999 | Polsar, 80 MHz | 0 | 60 |
| Runnels 180-1 | TS1162 | 5/21/1999 | XTI1p, 20 MHz | 180 | 60 |
| Runnels 360-2 | TS1163 | 5/21/1999 | XTI1p, 20 MHz | 0 | 60 |

oriented TOPSAR lines through the Montague site in July and October 1999 and for the Runnels site in October 1999 and December 2000.

We used the software ERMapper to convert the Stokes matrix polarimetry data to nonreferenced images of P- and L-band data in the HH, HV, and VV polarizations for the Runnels and Montague AIRSAR data sets. We also converted the C-band derivatives (digital elevation model, incidence angle, and VV polarization intensity) to nonreferenced images. These images were trimmed to the approximate boundaries of the Hatchel (Runnels County) and Prairie Valley School (Montague County) 7.5-minute quadrangles and were then georeferenced to digital 1-m resolution orthophoto quadrangle maps using ERMapper.

For detailed comparison with airborne EM data, we further trimmed the AIRSAR grids to the boundaries of the airborne EM surveys using the ArcView geographic information system to allow direct comparisons of radar reflectivity and measured ground conductivity patterns. We then selected specific airborne EM flight lines in each area that crossed notable salinization features, extracted the coordinates and apparent conductivity values measured along those lines, and then extracted the L- and P-band coordinates and polarimetry values falling within 5 m of the each airborne EM measurement location along the chosen lines.

Qualitative comparison of airborne EM and AIRSAR data was achieved by overlaying images of apparent conductivity as measured with the 56,000 Hz airborne induction coils with both individual C-, L-, and P-band polarizations and with composite images of P- and L-band polarimetry. Quantitative comparisons were made by plotting measured apparent conductivity and measured radar scattering intensity at various frequencies and polarizations against location along the chosen flight lines, and by calculating the correlation coefficient between measured apparent electrical conductivity and (a) all available radar frequencies and polarizations, and (b) all possible ratios of available radar frequencies and polarizations.

## RESULTS

Our approach in evaluating the usefulness of AIRSAR in mapping near-surface salinization was to qualitatively compare results from airborne EM surveys of the two test sites with individual and combined radar scattering images of the same areas and to quantitatively compare the results by extracting individual apparent conductivity measurements from select airborne EM flight lines and comparing those measurements to the nearest-neighbor radar backscatter using various combinations of radar frequency and polarization. We completed these comparisons for both the Hatchel and Montague Test Sites.

### Hatchel Test Site

The Hatchel Test Site, located in the Colorado River basin in West Texas (fig. 1), has been the subject of intensive investigation of the effectiveness of airborne geophysics in identifying near-surface salinization. We have used airborne EM to identify ground conductivity increases associated with salinization and have used airborne magnetics to identify oil and gas wells that are possible salinization sources. Results of the airborne survey and supporting ground-based geophysics and soil and water sampling are presented in numerous publications including Paine (1999), Paine and others (1997a and b), and Paine and others (1999). These studies demonstrated that there is a high correlation between ground conductivity and salinization, and that airborne EM accurately measures ground conductivity. We thus consider the apparent conductivity measured using airborne instruments at the highest frequency (shallowest exploration depth) to be the measurement with the greatest likelihood of corresponding to the electrical component of AIRSAR backscatter arising from near-surface interaction during the backscatter process. For AIRSAR to be effective in salinization mapping, there should be significant correlation between measured apparent conductivity and some AIRSAR backscatter component.

Hatchel Airborne EM Survey

Ground conductivity maps of the Hatchel Test Site (figs. 1 and 2) were produced after processing electromagnetic data acquired during the airborne survey (table 1; Garrie, 1996). Maps were made from horizontal coplanar induction coils operating at 56,000 (fig. 8), 7,200, and 900 Hz. Because exploration depth depends on both frequency and ground conductivity, deeper exploration depths were attained at lower coil frequencies and, for a given coil frequency, less conductive ground (fig. 7).

Grids of apparent ground conductivity measured at more than 157,000 locations by the 56,000 Hz coils, the shallowest exploration depth frequency, showed good contrast between the lowest observed values of about 60 to the highest values of 850 mS/m (fig. 8). Maximum exploration depths for this frequency deepen from 2.5 m over highly conductive ground to as much as 9 m over ground with the lowest observed conductivities (fig. 7). This depth range is the one that is most affected by near-surface changes in many factors that control ground conductivity, such as soil type (clay soils are more conductive than sandy soils), moisture content (wet soils are more conductive than dry soils), and water chemistry (saline water is more conductive than fresh water).

Highly conductive areas visible on the 56,000 Hz map include numerous small ovals that are generally 80 to 250 m across, curvilinear features that are a few hundred meters wide and hundreds of meters long, and large, irregularly-shaped features covering many square kilometers (fig. 8). Significant curvilinear features include (a) a zone about 200 m wide and more than 2 km long located along an east-facing bluff west of Bluff Creek in the northern part of the study area, (b) a segment about 400 m wide along Coyote Creek that extends from the northern edge of the study area to near the southern edge, (c) a 200-m wide zone along an east-facing bluff west of Elm Creek, and (d) a short segment of Elm Creek just downstream from its confluence with Eagle Branch (fig. 8). The most significant of the large, irregular areas of high conductivity are

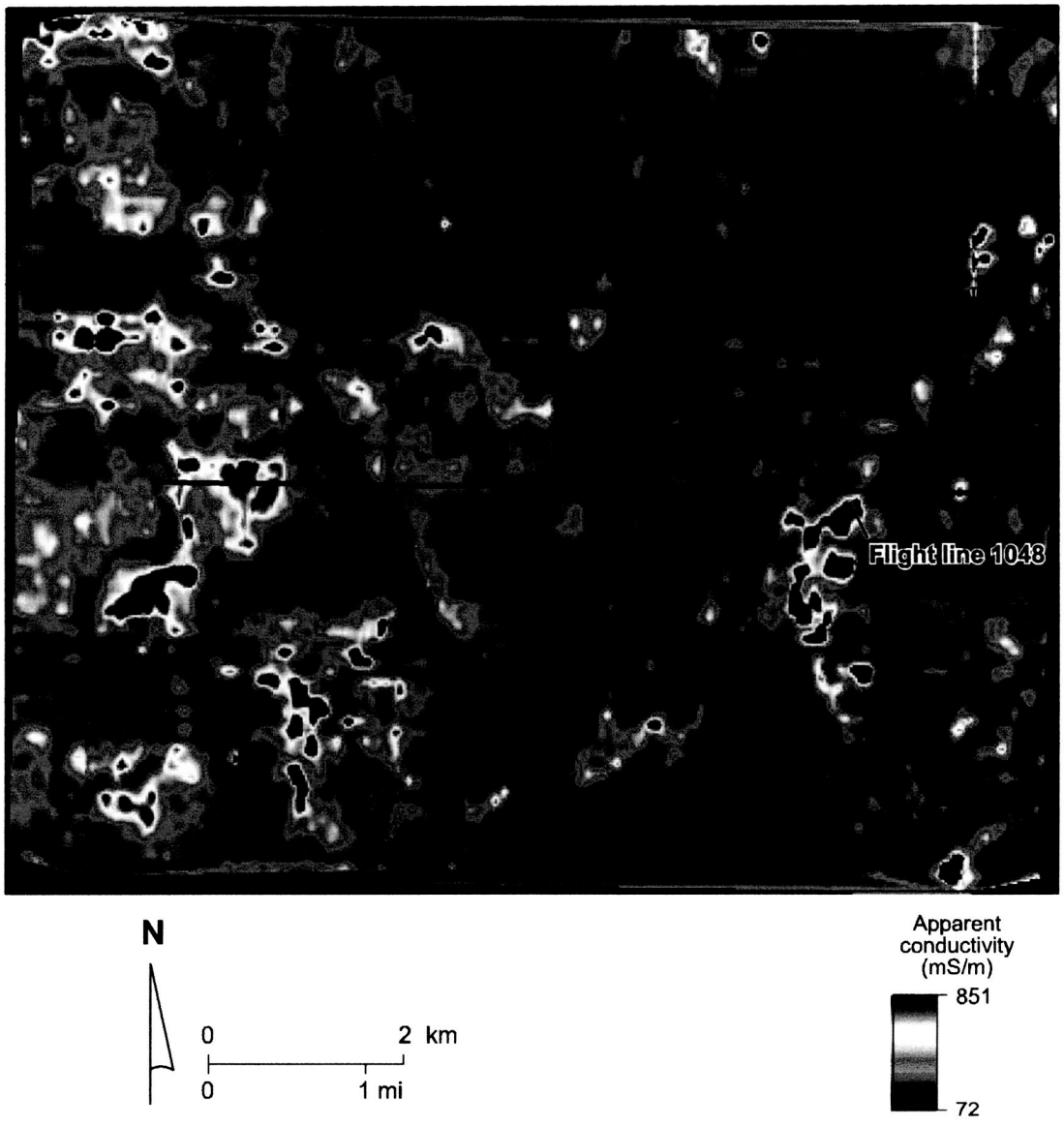


Figure 8. Apparent conductivity measured using 56,000 Hz airborne induction coils at the Hatchel Test Site, Runnels County, Texas (fig. 2). Also shown is the segment of airborne EM flight line 1048 used for detailed comparison with AIRSAR data.

(a) the western third of the study area, (b) an area south of Hatchel and east of Coyote Creek, and (c) the area just east of Elm Creek south of its confluence with Mud Creek (fig. 8).

Sites were chosen for detailed ground investigation (Paine and others, 1997a; Paine, 1999) largely from the smaller, oval-shaped anomalies because of the limited lateral distance that salt water plumes can move from brine pits and potentially leaking wells. These features also include small patches of conductive soil, springs, and stock tanks. The curvilinear conductivity highs located at similar elevations along a bluff or hill slope probably mark the location of ground water seeps where the land surface has intersected a water-bearing unit. Curvilinear features along the creeks most likely represent areas where higher salinity water flows in the creek or associated alluvium. The large, irregularly shaped features are too extensive to be caused by individual leaking wells, but some may be located where there are numerous closely spaced salt water sources. Most of these large features are probably not oilfield-related, but instead are located in areas where soils or shallow geologic units have more clay, are wetter, or contain water with higher dissolved mineral content.

## Runnels AIRSAR

Using TOPSAR data acquired in May 1999 during flight Runnels 180-1 (fig. 1 and table 3), we produced images of the Hatchel quadrangle depicting individual P- and L- band polarizations (figs. 9 and 10) and P- and L- band composites (fig. 11). C-band data were used to produce a digital elevation model (fig. 3). We used characteristic features visible on these 10-m resolution images to georeference the AIRSAR data to a 1-m resolution digital orthophotomosaic of the quadrangle and to qualitatively assess the applicability of AIRSAR to salinization mapping.

Backscatter amplitudes for the Hatchel quadrangle are about twice as high for the L-band polarizations than for the P-band polarizations. For both bands, backscatter amplitudes in the HH and VV polarization modes are about 10 times larger than those in the HV mode. For the P-band data, more than 99 percent of the backscatter values are below 0.01 in the HH and VV modes and

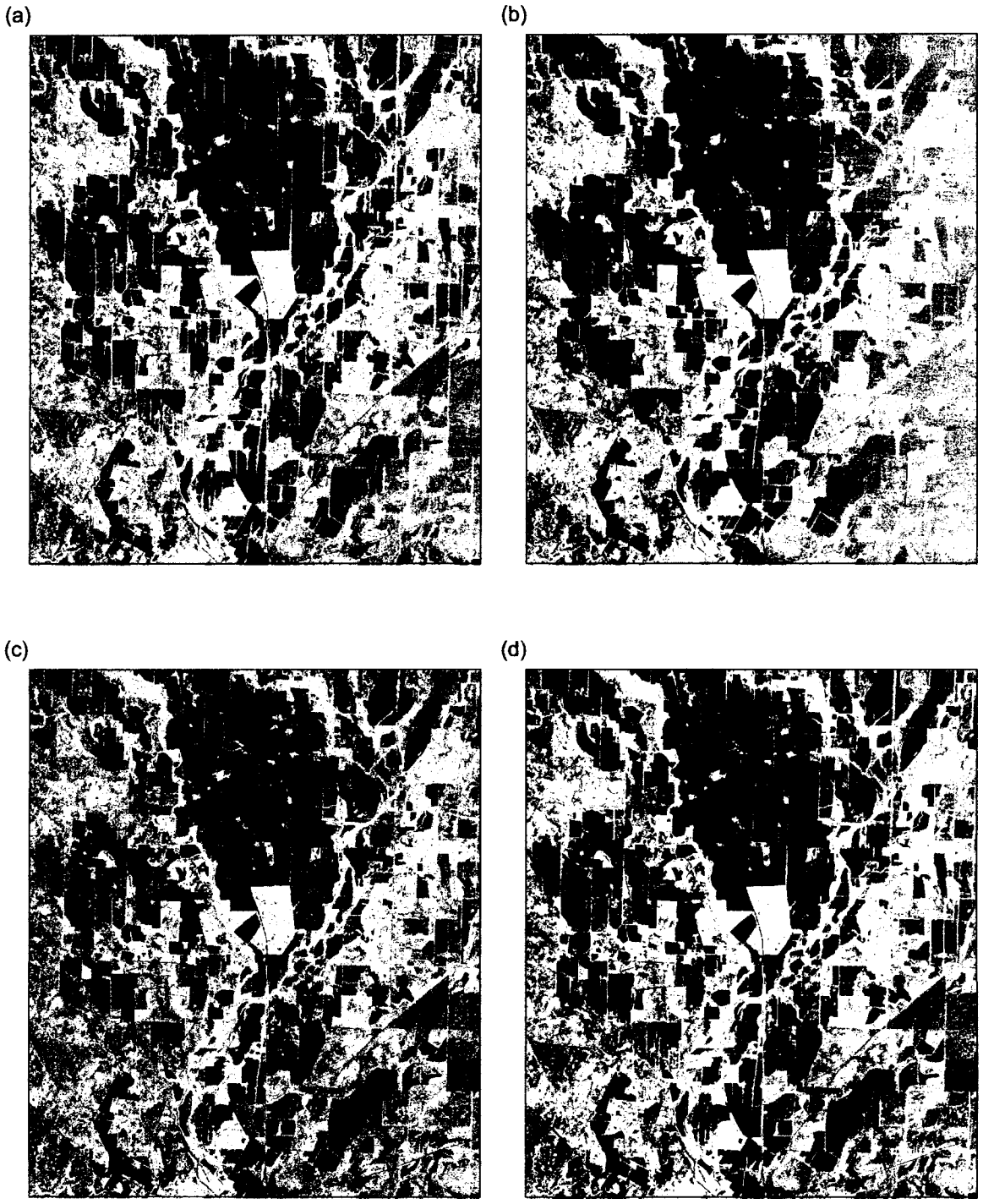


Figure 9. Georeferenced P-band radar backscatter for the Hatchel quadrangle (fig. 2), AIRSAR flight Runnels 180-1. (a) HH polarization; (b) HV polarization; (c) VV polarization; and (d) total power.

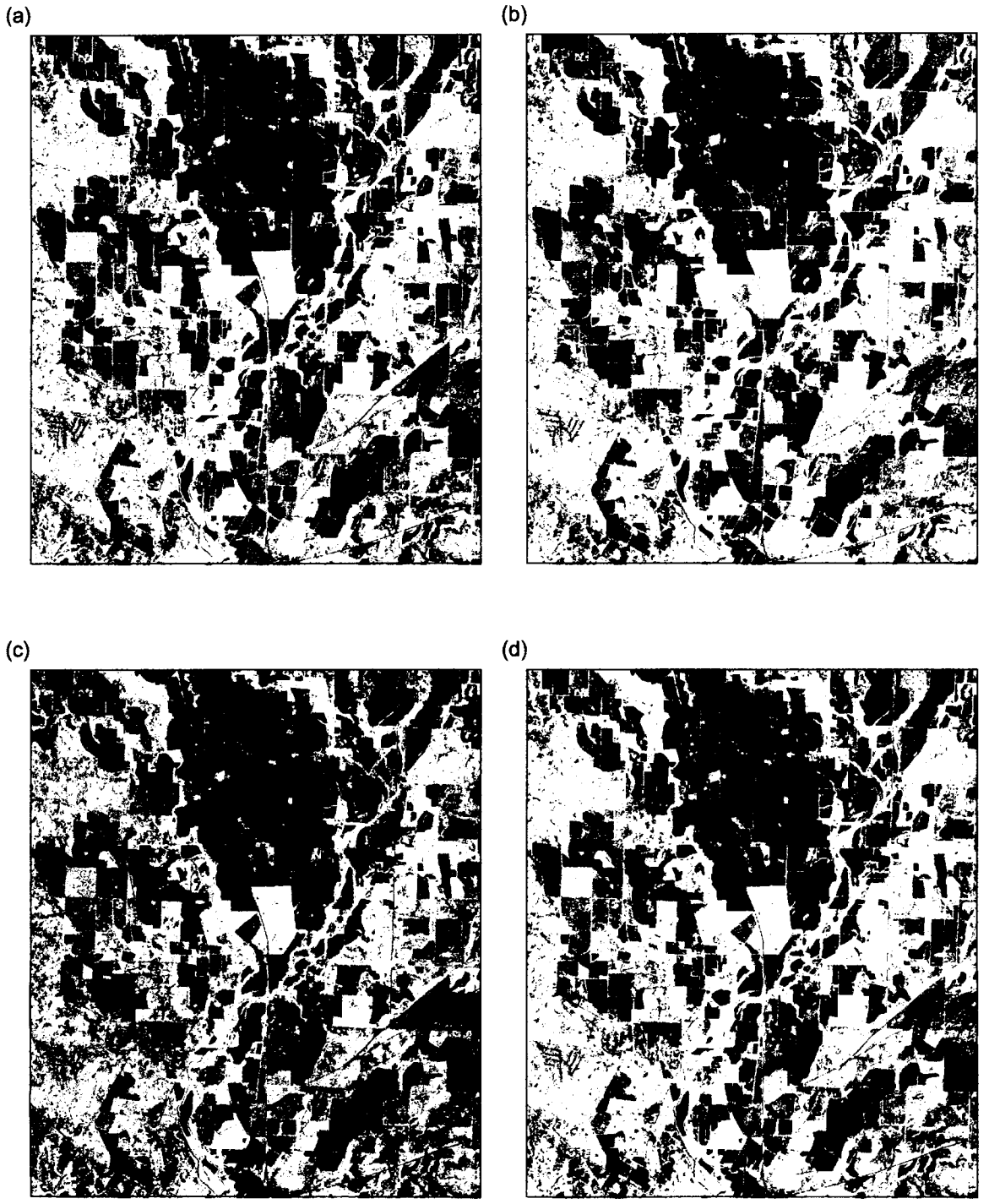


Figure 10. Georeferenced L-band radar backscatter for the Hatchel quadrangle, AIRSAR flight Runnels 180-1. (a) HH polarization; (b) HV polarization; (c) VV polarization; and (d) total power.

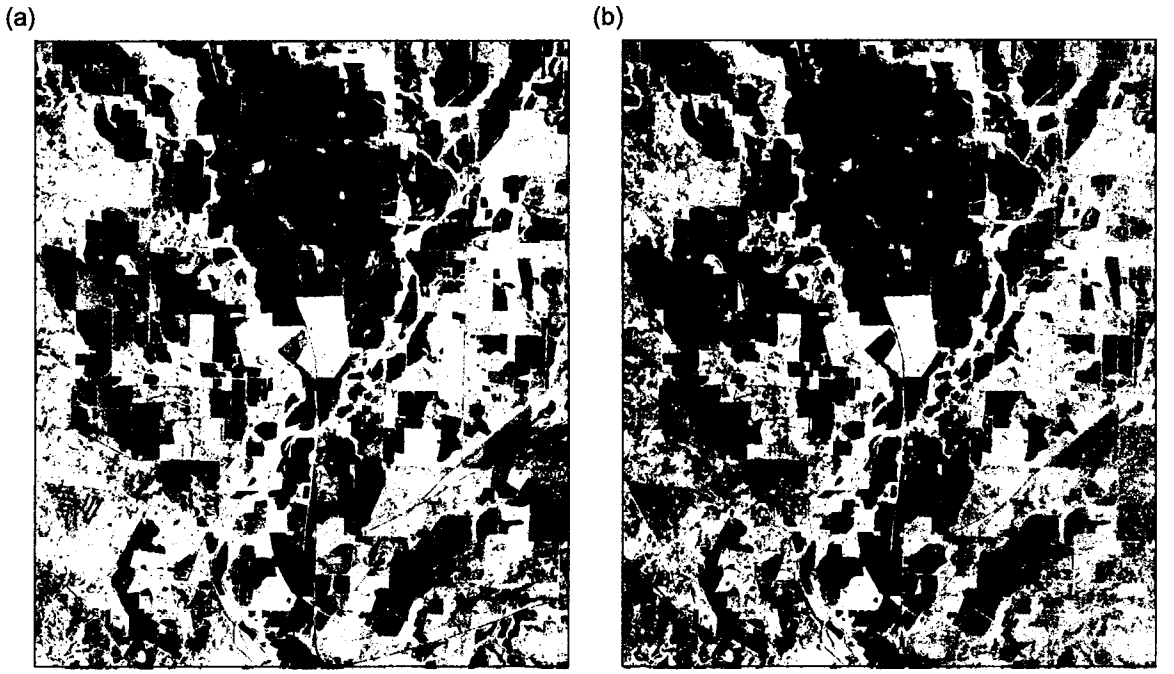


Figure 11. Georeferenced (a) L- and (b) P-band radar backscatter composites for the Hatchel quadrangle, AIRSAR flight Runnels 180-1. Composite images created using HH = red, HV = green, and VV = blue.

below 0.001 in the HV mode. For L-band, similar percentages of HH and VV values are below 0.021 and HV values are below 0.0014. The peak backscatter amplitudes in both P- and L-band data were recorded in HH mode; these locations correspond to metallic fences that are nearly parallel to the flight direction.

In both P- and L-band total power and individual polarization images, many surface features are well discriminated. Features readily discernible on these images include water bodies, agricultural fields in various stages of cultivation, vegetation changes along streams, power and fence lines, roads, and infrastructure associated with oil and gas development.

Composite images combining (a) the same polarization and differing radar frequencies and (b) the same frequency and differing polarizations are commonly used to discriminate among different types of sources of radar backscatter. With the P- and L-band polarimetry acquired in AIRSAR's TOPSAR mode, we constructed only P- and L-band composites of the Hatchel quadrangle (fig. 11). In these images, areas appearing red reflect relative HH-mode backscatter dominance, areas appearing green reflect relative HV-mode dominance, and areas appearing blue reflect relative VV-mode dominance. A strong red component (relative HH dominance) in L- (fig. 11a) and P- (fig. 11b) composites is visible along fences and power lines parallel to the flight direction, housing developments, and strongly contoured agricultural fields. A strong green component (relative HV dominance) is visible in the L composite in cultivated fields with mature grassy vegetation, and in the P composite in similar areas at relatively low incidence angles. Strong blue areas (relative VV dominance) are more prevalent on the P composite than on the L composite. In both bands, relative VV dominance is more common at high incidence angles and is found almost exclusively in cultivated fields. Tonal variations within these fields appear to match soil type variations visible on aerial photographs and aerial-photograph-based soil type maps (Wiedenfeld and others, 1970).

Qualitative comparisons of apparent conductivity patterns (figs. 12d and 13b) with VV backscatter in the C band (fig. 12a) and composite backscatter in the longer wavelength L and P bands (figs. 12b and c) and VV polarization composite backscatter (fig. 13a) reveal little system-

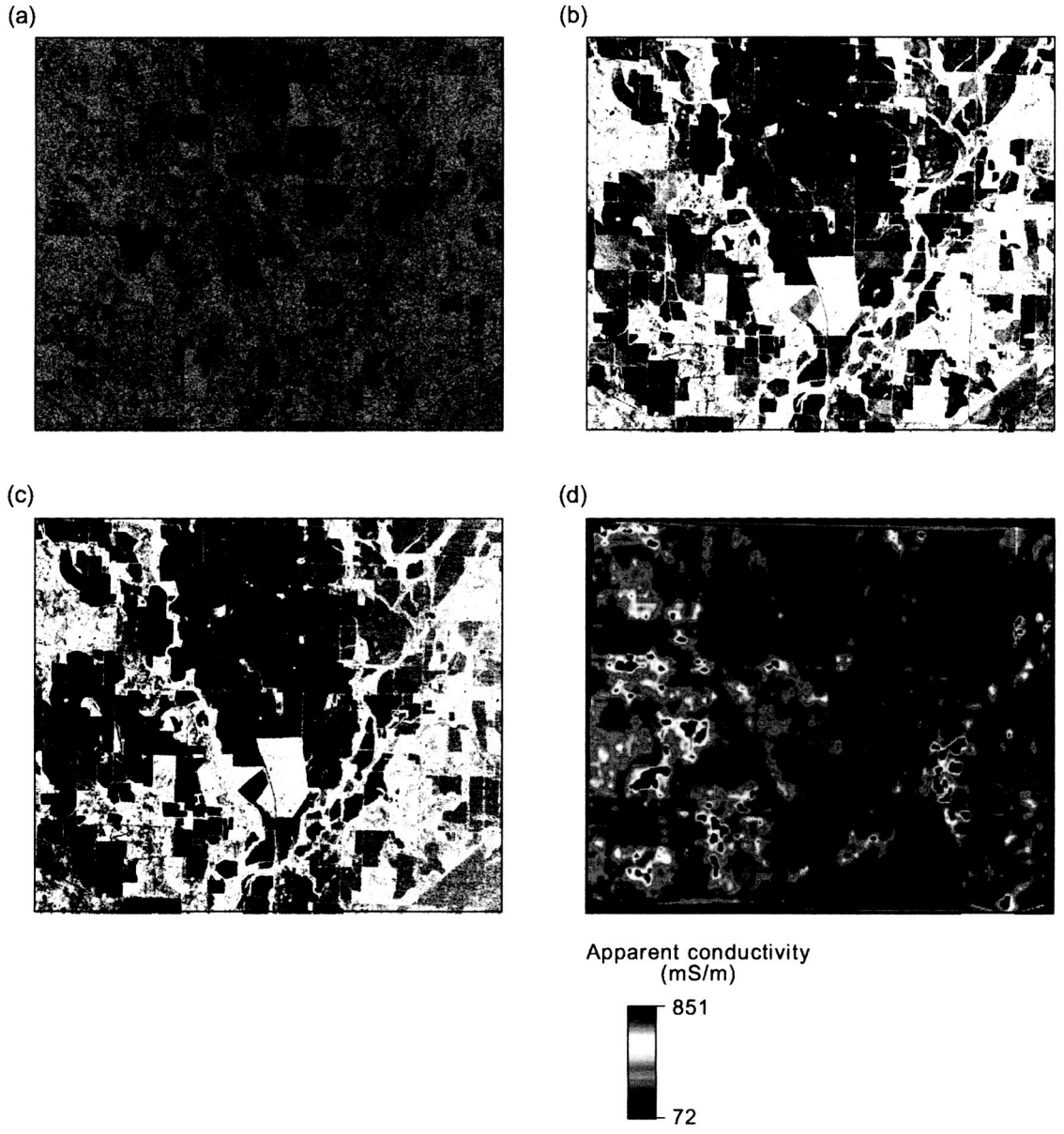


Figure 12. Co-registered images of radar backscatter for (a) C band (VV only); (b) L band (HH, HV, and VV composite); and (c) P band (HH, HV, and VV composite) and (d) apparent ground conductivity measured at 56,000 Hz at the Hatchel Test Site (fig. 2). Radar data from AIRSAR flight Runnels 180-1.

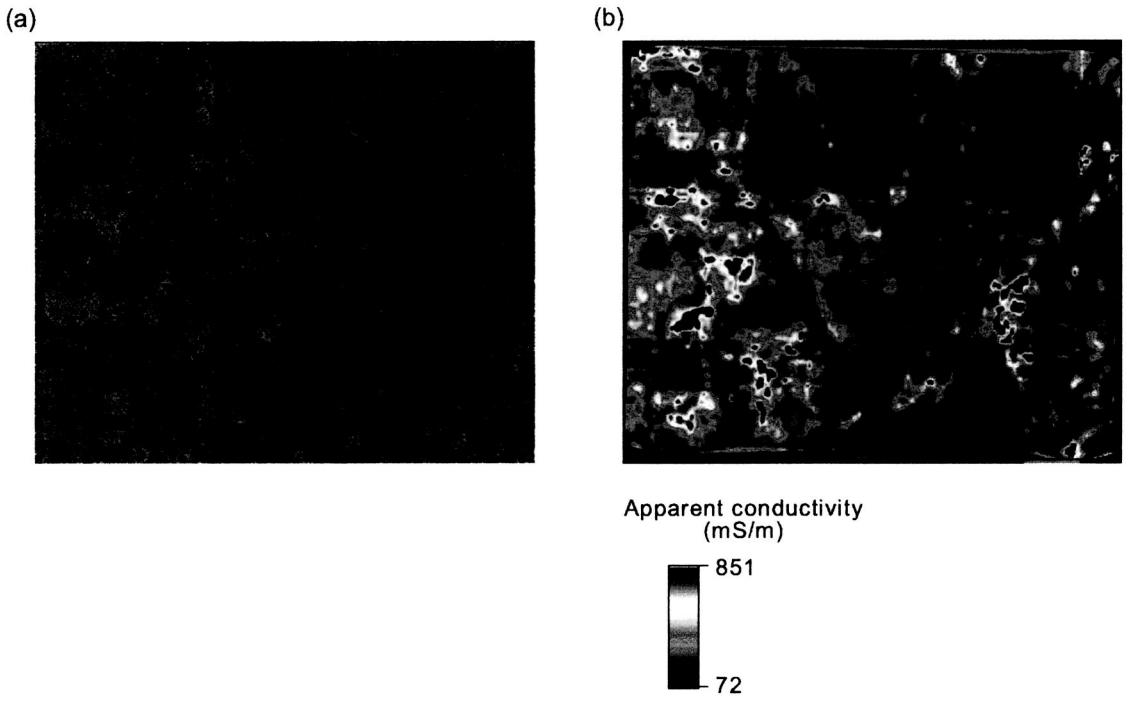


Figure 13. Co-registered images of the Hatchel Test Site created from (a) radar backscatter for VV polarization (C band = red, L band = green, and P band = blue) and (b) apparent ground conductivity measured at 56,000 Hz. Radar data from AIRSAR flight Runnels 180-1.

atic similarity at the Hatchel Test Site. Radar backscatter patterns at all frequencies are dominated by land use patterns, allowing ready discernment of cultivated field boundaries, streams, fences, power lines, and roads. Conductivity patterns are dominated by soil and rock distribution trends, soil moisture changes, and pore water chemistry variations that can be modified by land use.

We compared measured apparent conductivity and radar backscatter more quantitatively by (1) selecting a representative flight line from the airborne EM data set (line 1048, fig. 8), (2) extracting the original, ungridded apparent conductivity measurements made using 56,000 Hz airborne induction coils, (3) overlaying those measurement points on AIRSAR backscatter grids, and (4) extracting backscatter measurements at all available frequencies and polarizations at locations within 5 m of an apparent conductivity measurement. We then looked for similarities in response by plotting conductivity and backscatter signals with distance along the flight line and by plotting co-located conductivity and backscatter signals and calculating correlation coefficients.

Apparent conductivity values measured along Hatchel flight line 1048 cross several physiographic features and reasonably capture the variability from heavily salinized to nonsalinized ground. Apparent conductivity measured at 876 locations along this line averages 286 mS/m, ranging from 102 to 989 mS/m (fig. 14). Highest apparent conductivities are found on the western part of the line. Neither the strong P-band backscatter in HH and VV polarizations (fig. 14a and c) nor the weaker cross polarization backscatter (HV, fig. 14b) are spatially well correlated to apparent conductivity. Plots of radar backscatter intensity and apparent conductivity suggest a decrease in radar backscatter as apparent conductivity increases (fig. 15), particularly for VV polarization and cross polarization. This small negative correlation is reflected in correlation coefficients of –0.14 for VV and –0.18 for HV and near 0 for HH (table 4).

Similarly, L-band backscatter intensities for individual polarizations show little spatial correlation with apparent conductivity (fig. 16), but exhibit a slight negative correlation between backscatter intensity and conductivity as conductivity increases (fig. 17). Correlation coefficient

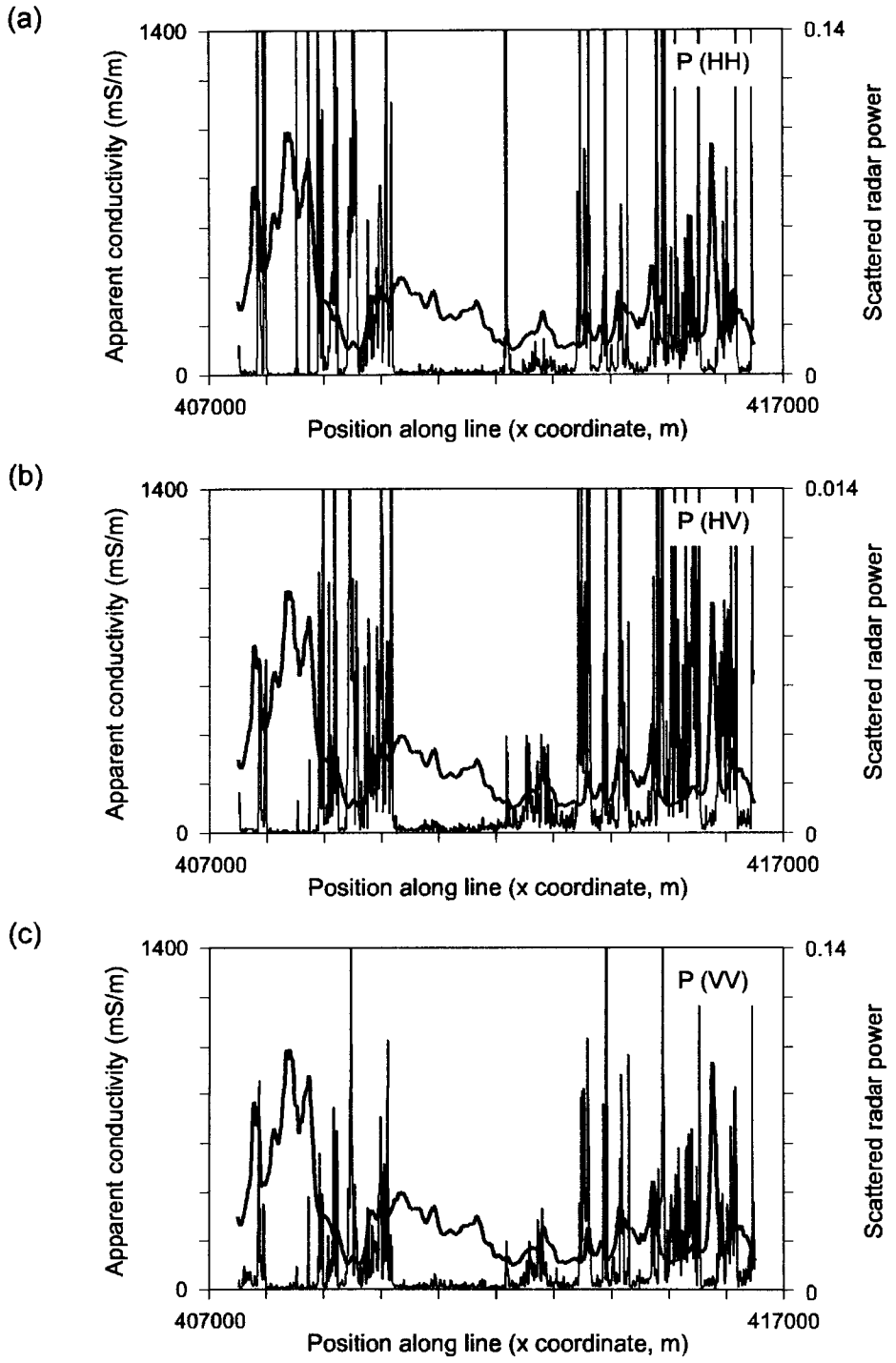


Figure 14. Comparison of P-band backscatter and apparent conductivity measured along Hatchel flight line 1048 (fig. 8) in the (a) HH, (b) HV, and (c) VV polarizations.

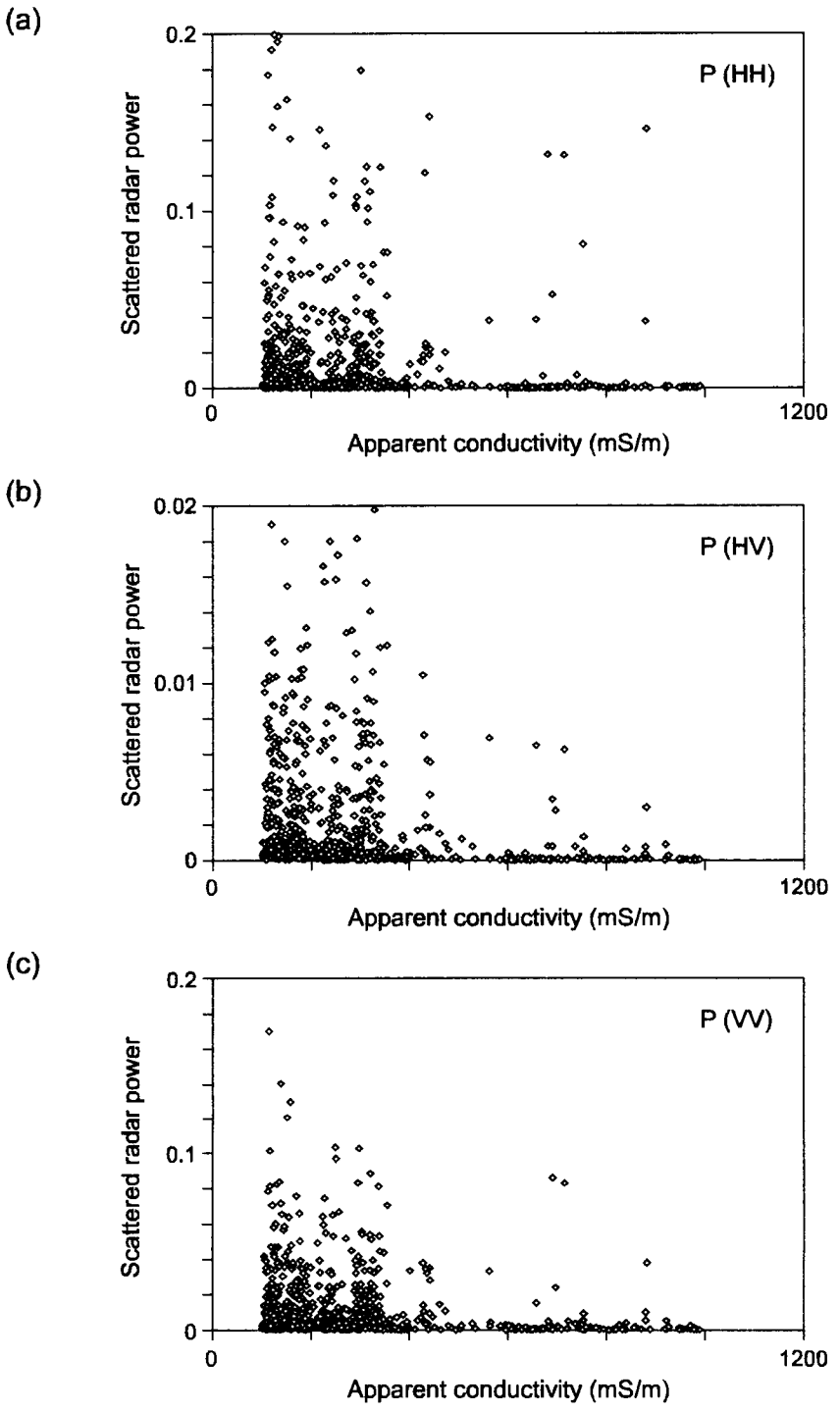


Figure 15. Relationship between apparent conductivity and P-band backscatter in (a) HH, (b) HV, and (c) VV polarizations along Hatchel flight line 1048.

Table 4. Correlation coefficients calculated between apparent conductivity values measured using airborne induction coils operating at 56,000 Hz and the measured radar reflectance or reflectance ratios at points within 5 m of the conductivity measurement location.

| **Parameter or ratio** | **Montague line 10210** | **Runnels line 1048** |
|---|---|---|
| PVV | -0.107 | -0.136 |
| PHV | -0.139 | -0.177 |
| PHH | -0.014 | -0.059 |
| LVV | -0.105 | -0.143 |
| LHV | -0.091 | -0.148 |
| LHH | -0.034 | -0.087 |
| PVV/PHV | 0.037 | 0.314 |
| PVV/PHH | -0.026 | 0.051 |
| PVV/LVV | -0.012 | -0.079 |
| PVV/LHV | 0.065 | 0.322 |
| PVV/LHH | -0.003 | -0.048 |
| PHV/PHH | -0.097 | -0.119 |
| PHV/LVV | -0.036 | -0.161 |
| PHV/LHV | 0.068 | -0.038 |
| PHV/LHH | -0.078 | -0.185 |
| PHH/LVV | -0.032 | -0.030 |
| PHH/LHV | -0.026 | 0.013 |
| PHH/LHH | -0.020 | -0.063 |
| LVV/LHV | 0.094 | 0.388 |
| LVV/LHH | -0.017 | -0.013 |
| LHV/LHH | -0.122 | -0.227 |

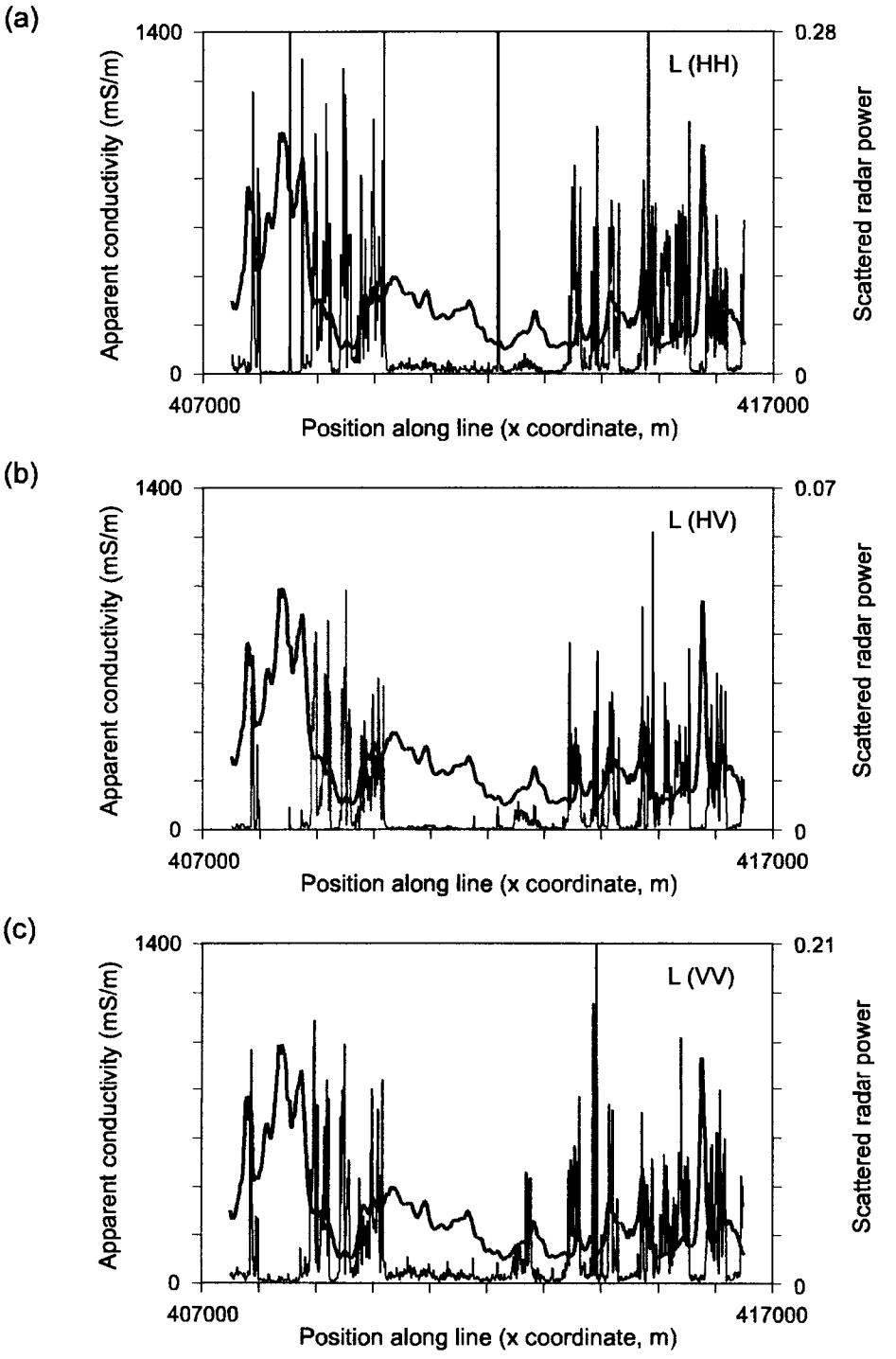


Figure 16. Comparison of L-band backscatter and apparent conductivity measured along Hatchel flight line 1048 in the (a) HH, (b) HV, and (c) VV polarizations.

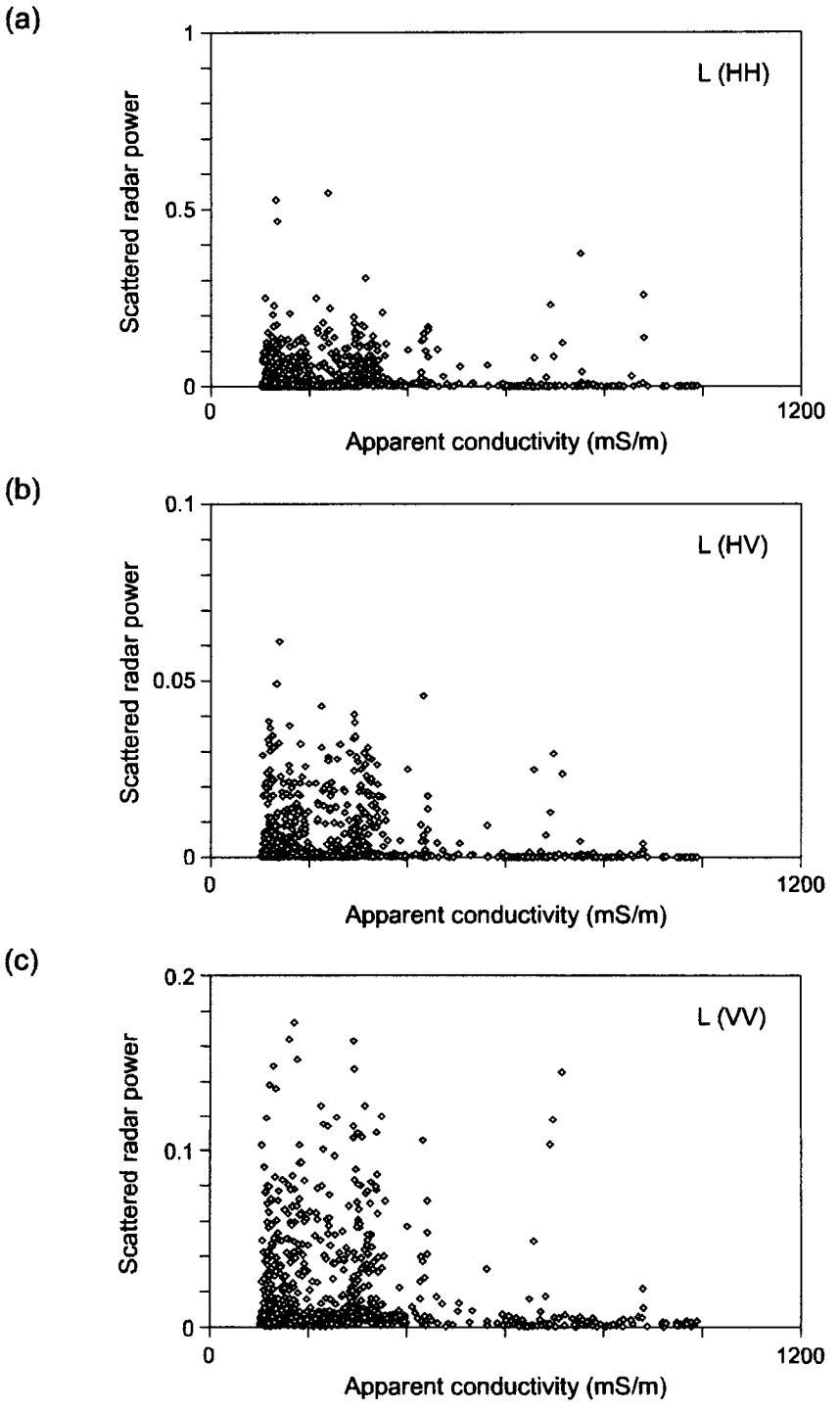


Figure 17. Relationship between apparent conductivity and L-band backscatter in (a) HH, (b) HV, and (c) VV polarizations along Hatchel flight line 1048.

magnitudes remain low, but are again greatest for HV (-0.148) and VV (-0.143) polarizations (table 4). Possible causes for this effect in both P- and L-band data include the known correlation between salinization intensity, ground conductivity, and barren ground and the limited radar backscatter from barren ground.

Better correlation between radar backscatter and apparent conductivity is achieved when differing radar bands and polarizations are combined in an attempt to enhance the effect of the near-surface electrical properties on radar backscatter. For example, we expect that the longer wavelength of the P-band signal will interact proportionately more with soil than will the shorter wavelength L-band signal, making it possible to enhance the electrical component by calculating the ratio of the two signals. Although ratios calculated from data along Hatchel line 1048 produce poor correlations for most possible band and polarization combinations, a few did produce positive correlations above 0.3 (table 4). The highest of these (0.388) was the ratio of the L-band VV polarization to the L-band cross polarization, which exhibits reasonable spatial correlation with apparent conductivity along the line (fig. 18a) and a discernible increase as apparent electrical conductivity increases (fig. 19a). The ratio calculated using these polarizations for the P-band data also exhibited relatively good correlation with apparent conductivity (figs. 18c and 19c), as did the ratio of P-band VV polarization to L-band cross polarization (figs. 18b and 19b). The only other ratio with a correlation magnitude above 0.2 was the L-band cross polarization to L-band HH polarization combination (table 4), which had a slight negative correlation.

## Montague Test Site

The Montague Test Site is located in North Texas adjacent to the Red River (figs. 1 and 4). We employed several EM methods at the Montague site to address different aspects of salinization. In contrast to the Hatchel Test Site, a larger area where numerous old oilfields and natural sources of salinization exist, the Montague Test Site encompasses a single oil field associated with a large, shallow saline-water plume that has impacted surface water, ground water, and

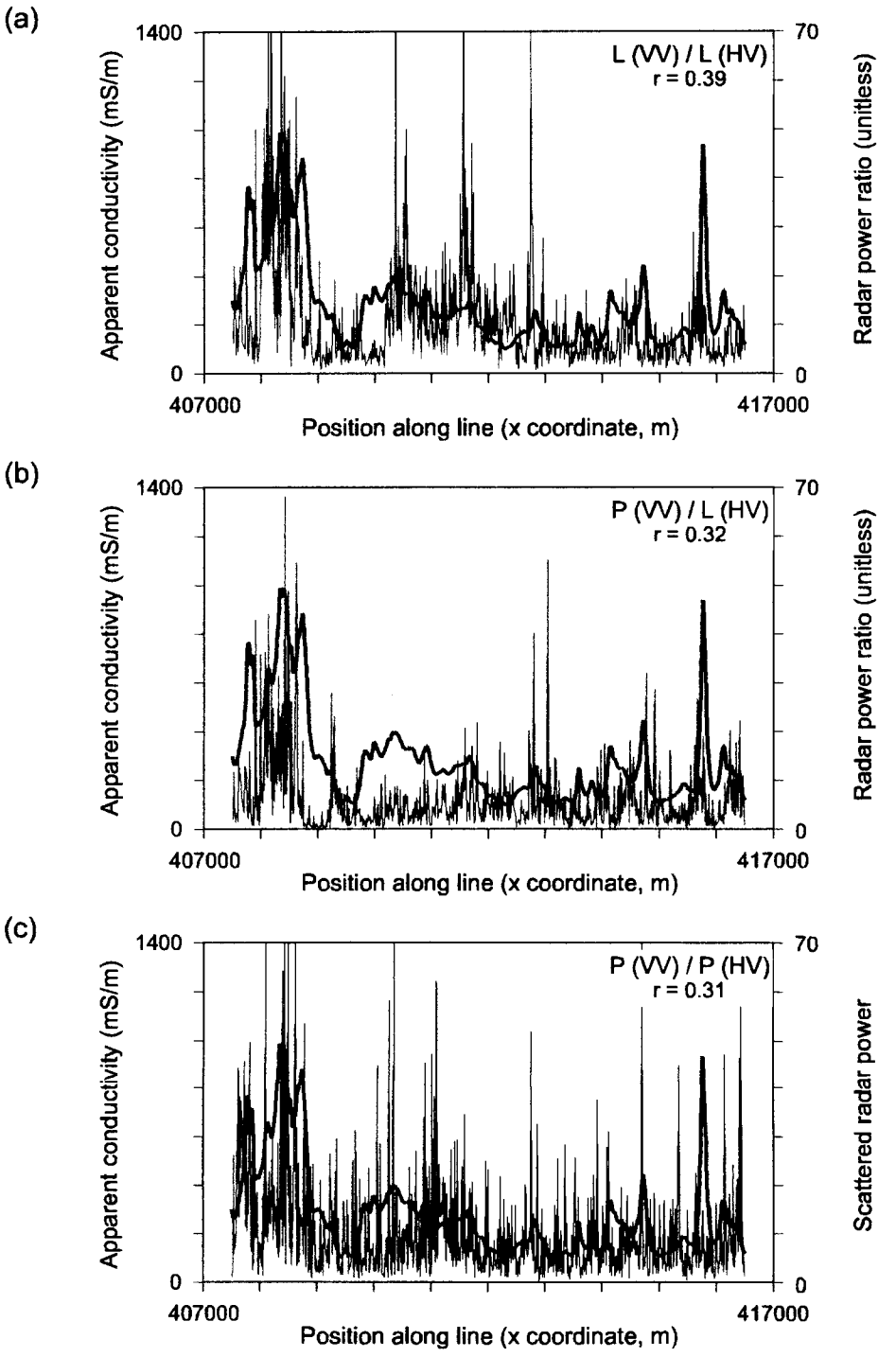


Figure 18. Comparison of radar backscatter ratios and apparent conductivity measured along Hatchel flight line 1048. The ratios with the three highest correlation coefficients are shown.

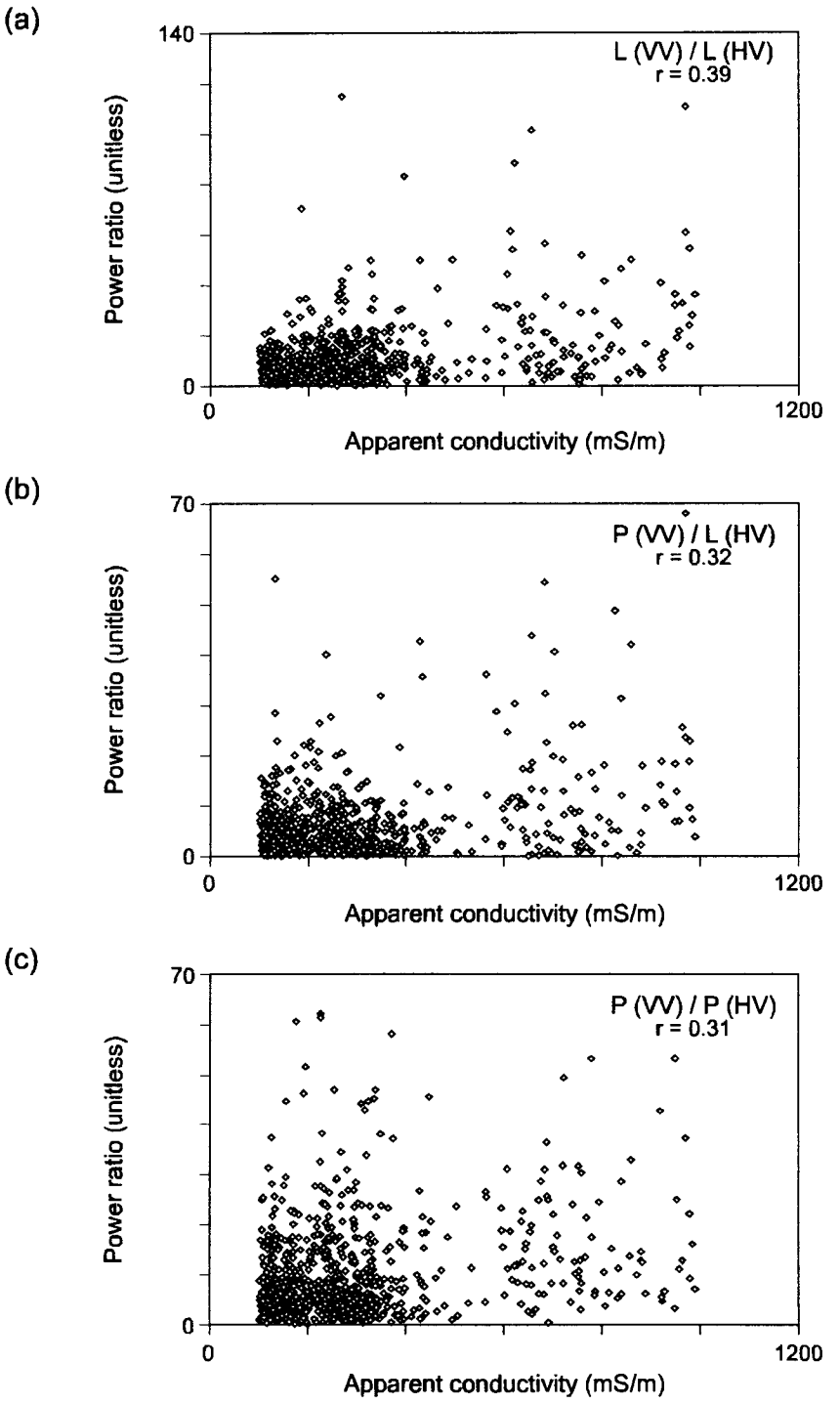


Figure 19. Relationship between apparent conductivity and radar backscatter ratios along Hatchel flight line 1048. The ratios with the three highest correlation coefficients are shown.

agriculture in the area. Reconnaissance ground-based EM measurements established the boundaries of the salinized area, suggested the presence of multiple salinity sources, and determined the range of electrical conductivity observed at the site. Airborne conductivity measurements established the relative intensity and lateral extent of salinization, located potential salinity sources, and were used to optimize borehole locations. Borehole measurements and time-domain EM soundings determined the vertical extent of salinization and helped established the relationship between ground conductivity and chloride content. We then used the airborne EM data and the empirical relationship between chloride content and electrical conductivity in water to estimate total mass of chloride present in the Montague salt-water plume. Salinization research at this site is summarized in Collins and others (1999), Hovorka and others (1999), and Paine (2003). The AIRSAR mission over the Montague Test Site was flown in May 1999 to explore whether discrete salinization sources and discharge areas identified in the geophysical studies could be detected using airborne radar.

## Montague Airborne EM Survey

Reconnaissance measurements obtained with a ground conductivity meter across the Montague site (Hovorka and others, 1999) revealed that apparent conductivities ranged from less than 50 mS/m in areas with no evidence of salinization to 200 mS/m or more across salt-water seeps and barren areas. These surveys also indicated that (1) there is a conductivity anomaly associated with the barren area on the Pleistocene terrace of the Red River (figs. 4 and 5), (2) the conductivity anomaly underlies an area that is much larger than the barren area, (3) several conductivity anomalies exist along the streams that cross the oil field south of the terrace (fig. 4), suggesting multiple sources of saline water, and (4) the salinity sources and salinization are bounded by an area that is about 4.5 km east–west by about 5.5 km north–south. This area was subsequently surveyed with airborne EM instruments.

Maps of ground conductivity, as measured by the airborne 56,000, 7,200, and 900 Hz induction coils, are similar and clearly show the extent of highly conductive ground (fig. 20). Exploration depths for the 56,000-Hz coils, calculated from the known frequency and from the observed conductivity range of 25 to 3,000 mS/m, range from about 1 m for the most conductive ground to about 14 m for the least conductive ground (fig. 7).

Particularly at high EM frequencies, many conductivity anomalies in the oil field on the Permian upland coincide with known brine-pit locations obtained from aerial photographs taken in 1966 before pit closure. Each of these anomalies is several hundred meters across and shows greater connection with adjacent anomalies and with the large anomaly on the Pleistocene terrace as EM exploration depth increases. A large salinized area on the Pleistocene terrace is barren of vegetation and falls within a larger conductivity anomaly that has conductivities ranging from just above background values (about 50 mS/m) to the highest conductivities observed for each frequency. This large anomaly has a sharp eastern boundary that may be controlled by paleotopography on the buried Permian surface, a bifurcation into a northeast-trending branch and a west-trending branch that intersects the Red River, and a diffuse northern boundary (fig. 20). Parts of the modern floodplain of the Red River, and the Red River itself, are also highly conductive, reflecting the naturally high salinity in the river and its alluvium.

Because the shape of the area characterized by above-background conductivities is irregular, we calculated the total area of conductive ground related likely to be related to Montague-site salinization by (1) drawing a boundary around the area that excluded highly conductive areas outside of the salt-water plume that originates in the upland oil field and (2) calculating a conductivity distribution for the area inside the boundary. Including both the Pleistocene terrace and Permian upland, 10.1 $km^2$ is underlain by ground with an apparent electrical conductivity greater than 70 mS/m. Conductive areas outside the boundaries of this plume, such as those visible in the northwest and southwest parts of the airborne survey (fig. 20), are likely to be caused by other natural and oil-field salinity sources in Texas and Oklahoma.


Figure 20. Apparent conductivity measured using 56,000 Hz airborne induction coils at the Montague Test Site, Montague County, Texas (fig. 4). Also shown is the segment of airborne EM flight line 10210 used for detailed comparison with AIRSAR data.

Montague AIRSAR

Using TOPSAR data acquired in May 1999 during flight Montague 180-1 (fig. 1 and table 3), we produced images of the Prairie Valley School quadrangle depicting individual P- and L- band polarizations (figs. 21 and 22) and P- and L- band composites (fig. 23). C-band data were used to produce a digital elevation model (fig. 5). We used characteristic features visible on these 10-m resolution images to georeference the AIRSAR data to a 1-m resolution digital orthophotomosaic of the quadrangle and to qualitatively assess the applicability of AIRSAR to salinization mapping.

For the individual P-band polarization images of the entire Prairie Valley School quadrangle, the HH (fig. 21a) and VV (fig. 21c) backscatter amplitudes are similar to those measured for the Hatchel quadrangle. More than 99 percent of the backscatter values are 0.01 or less, which is the same as the range for Hatchel and is about an order of magnitude higher than the 0.0012 range limit for the cross-polarized P-band backscatter (fig. 21b). The largest backscatter response is produced in the HH mode by fences that are parallel to the flight line. The Red River, Lake Nocona, and some barren areas have no backscatter response in HH, HV, or VV mode.

At the quadrangle scale, backscatter response in HH, HV, and VV polarization is similar in the L and P bands (figs. 21 and 22). As was also true for the Hatchel quadrangle, Prairie Valley School quadrangle backscatter values in all polarization modes are about 50 percent higher in L band than they are in P band; 99 percent of L-band HH and VV values are below 0.016 and HV values are below 0.0016. The strongest L-band backscatter is in the HH polarization and corresponds with fences oriented parallel to the flight line. L-band backscatter data show a strong spatial correlation with land-use patterns. Cultivated fields, developed areas, and vegetation density changes are all easily discernible on L- as well as P-band images of the Prairie Valley School quadrangle.

Composite images of the Prairie Valley School quadrangle constructed from L- and P-band polarimetry (fig. 23) show color variations reflecting the relative dominance of HH (red), HV

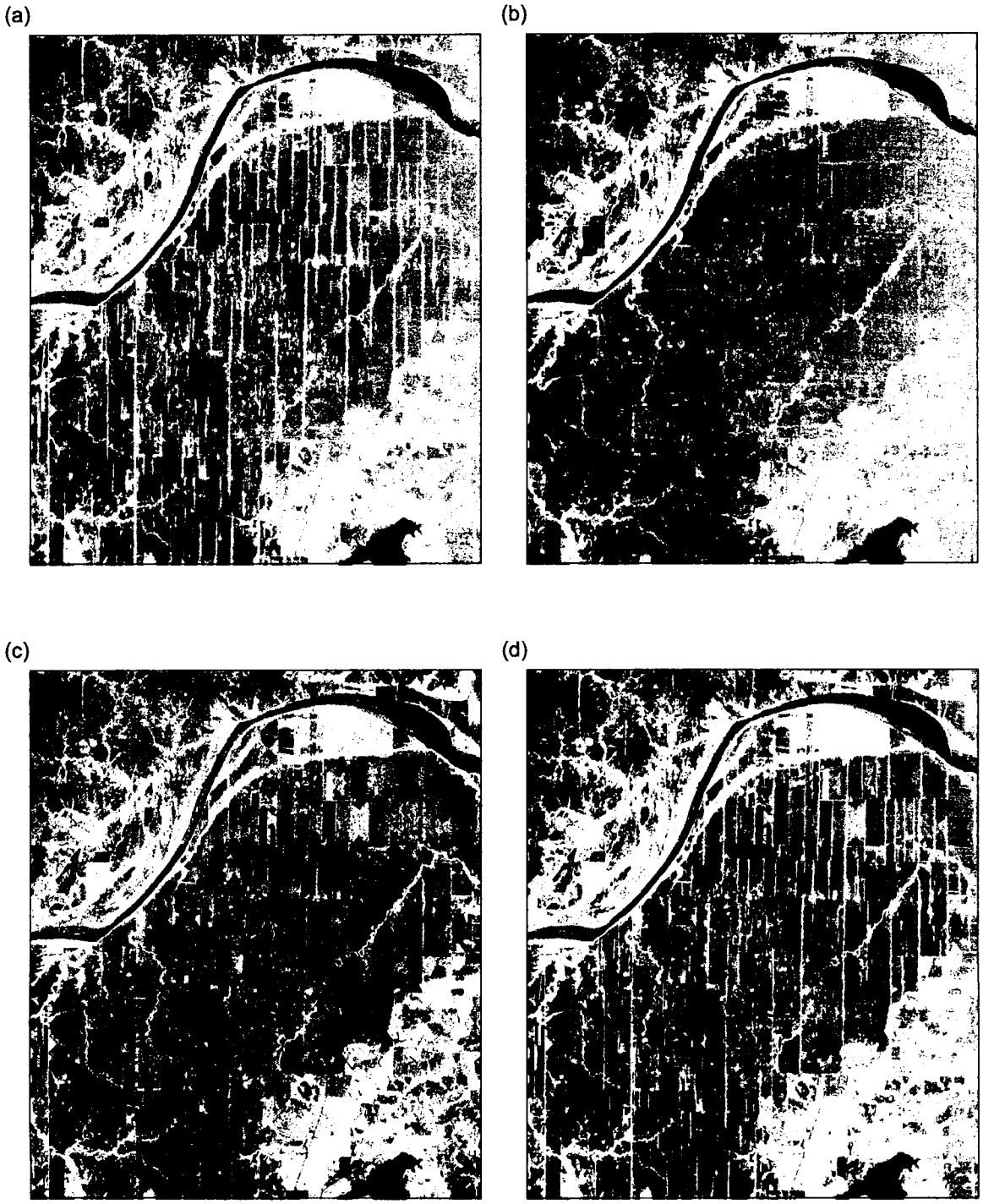


Figure 21. Georeferenced P-band radar backscatter for the Prairie Valley School quadrangle (fig. 4), AIRSAR flight Montague 180-1. (a) HH polarization; (b) HV polarization; (c) VV polarization; and (d) total power.

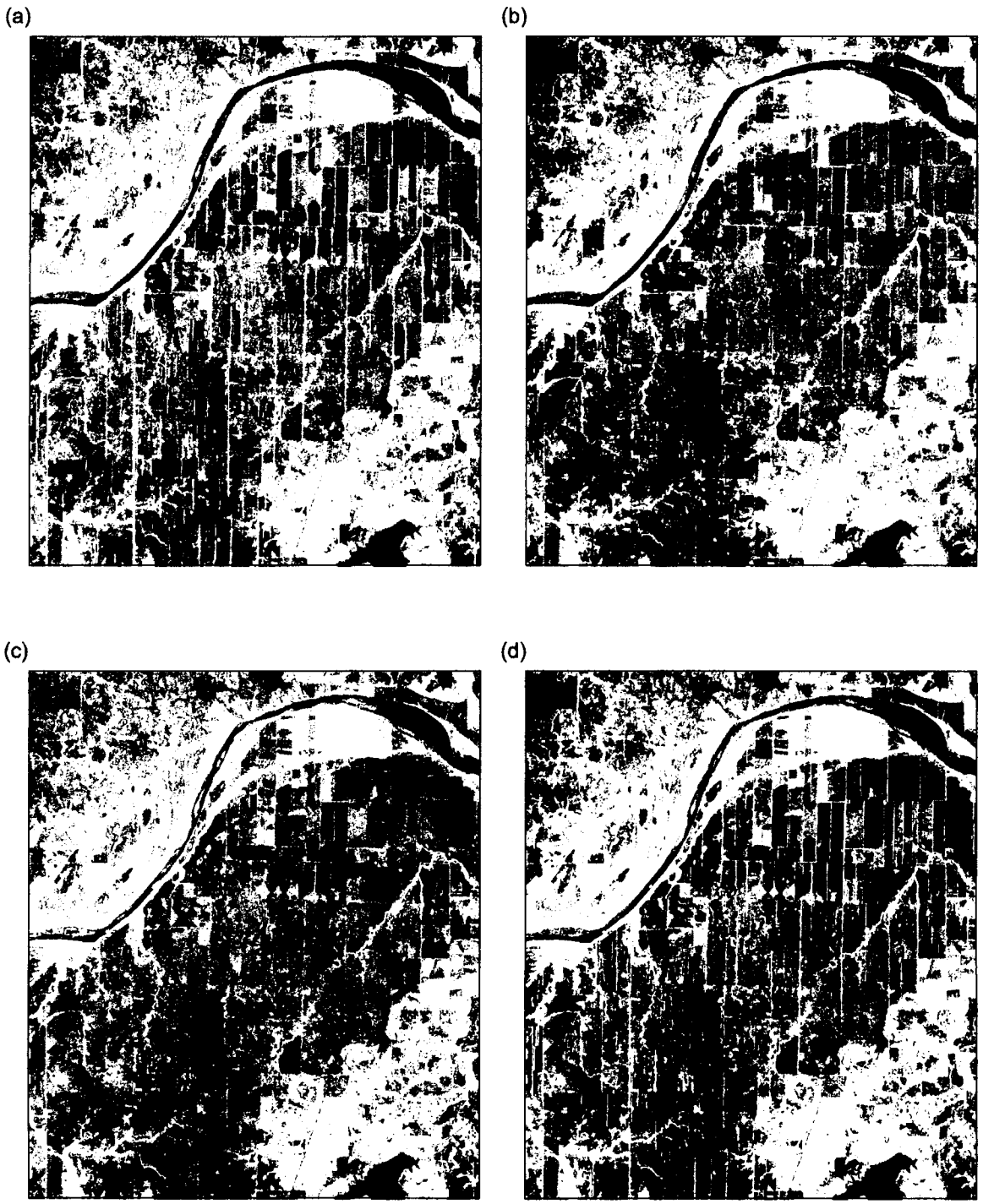


Figure 22. Georeferenced L-band radar backscatter for the Prairie Valley School quadrangle, AIRSAR flight Montague 180-1. (a) HH polarization; (b) HV polarization; (c) VV polarization; and (d) total power.

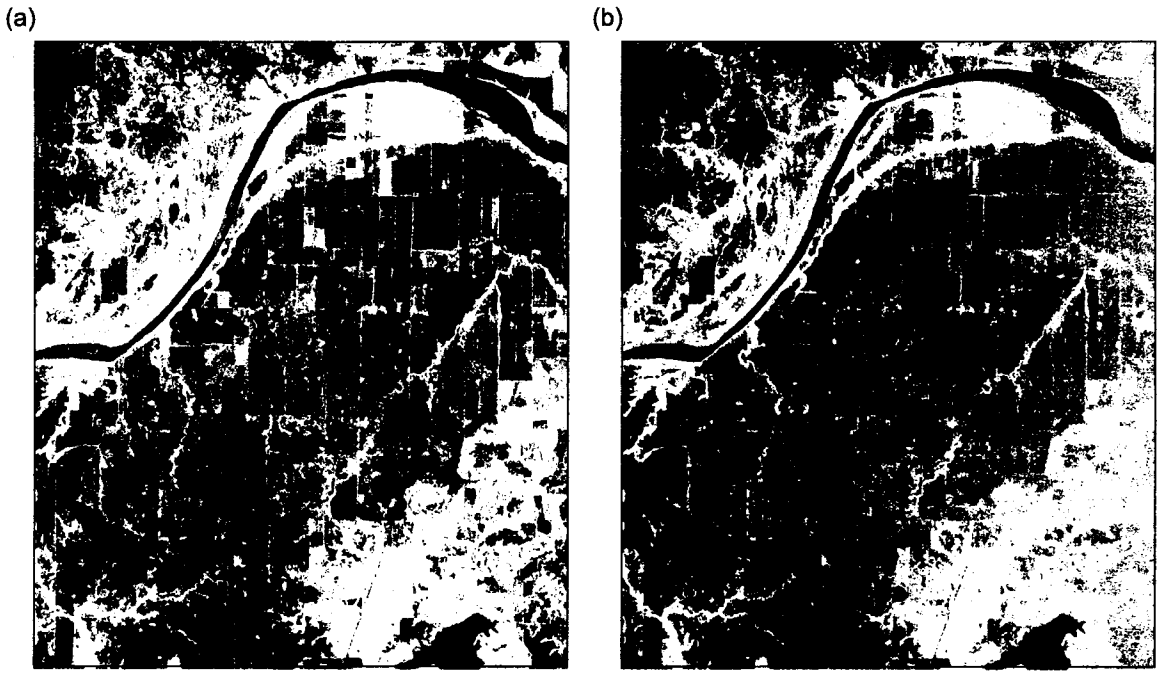


Figure 23. Georeferenced (a) L- and (b) P-band radar backscatter composites for the Prairie Valley School quadrangle, AIRSAR flight Montague 180-1. Composite images created using HH = red, HV = green, and VV = blue.

(green), or VV (blue) backscatter. In the L-band data (fig. 23a), HH mode (red) dominates along fences and power lines and across some cultivated fields with low vegetation. HV mode backscatter (green) dominates in some cultivated fields, along several fences oriented at an oblique angle to the flight line, and along small drainages with slightly denser vegetation than the surrounding cultivated fields. VV mode (blue) dominates in interchannel sandy areas along the Red River and some cultivated fields with relatively tall vegetation. P-band polarization dominance trends are similar (fig. 23b); HH mode correlates well to fence and power lines, HV mode is relatively strong in cleared areas of low or sparse vegetation, and VV mode backscatter is relatively strong in interchannel sandy areas of the Red River and some cultivated fields with tall vegetation.

We used subsets of the Prairie Valley School quadrangle AIRSAR data to create co-registered radar images that coincide with the Montague airborne EM survey boundaries (figs. 24 and 25). The C-band image (fig. 24a), showing VV polarization mode only, displays strongest backscatter along the Red River, in some cultivated fields, and from oilfield and agricultural infrastructure. The barren area associated with the salinity plume coincides with an area of no backscatter, as does the Red River channel. L- and P-band composites constructed from HH, HV, and VV data also indicate no backscatter from the barren area near the center of the salinity plume on the Pleistocene terrace (figs. 24b and c).

The VV composite image of the Montague Test Site constructed from C- (red), L- (green), and P- (blue) band data (fig. 25a) depicts relative C dominance in some cultivated areas, relative L dominance along the main channel of the Red River, and relative P dominance in some parts of cultivated fields where C backscatter dominates in other parts of the same field, depending on orientation of the crop rows. Neither the C-, L-, or P-band composite images nor the VV multiband composite appear to correlate spatially with apparent conductivity measured using the 56,000 Hz airborne induction coils (figs. 24d and 25b); instead, they appear to spatially correlate best with land use patterns and infrastructure such as cultivated fields, cleared land, fence and power lines, and residential, agricultural, and oilfield structures.

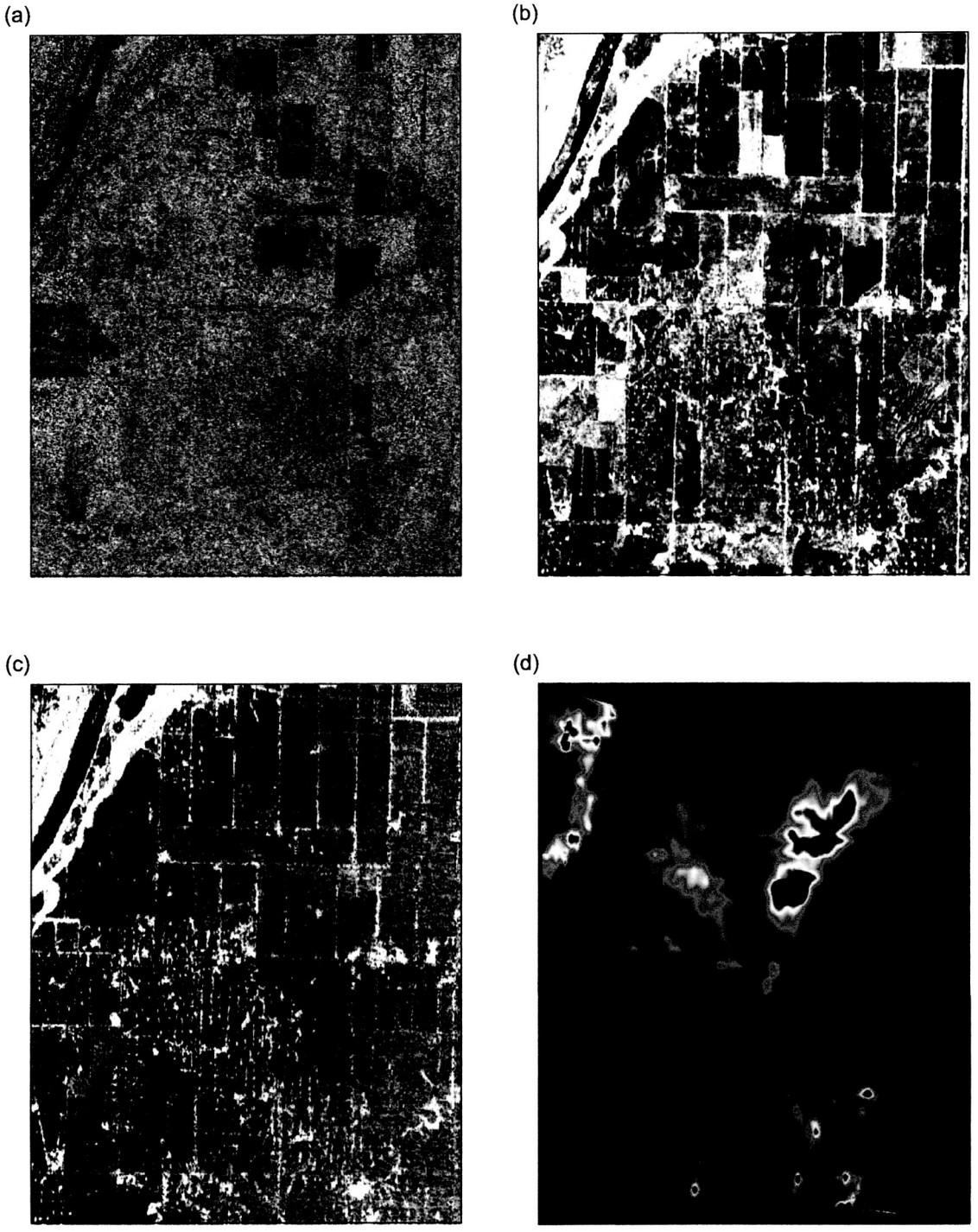


Figure 24. Co-registered images of radar backscatter for (a) C band (VV only); (b) L band (HH, HV, and VV composite); and (c) P band (HH, HV, and VV composite) and (d) apparent ground conductivity measured at 56,000 Hz at the Montague Test Site (fig. 2). Radar data from AIRSAR flight Montague 180-1.

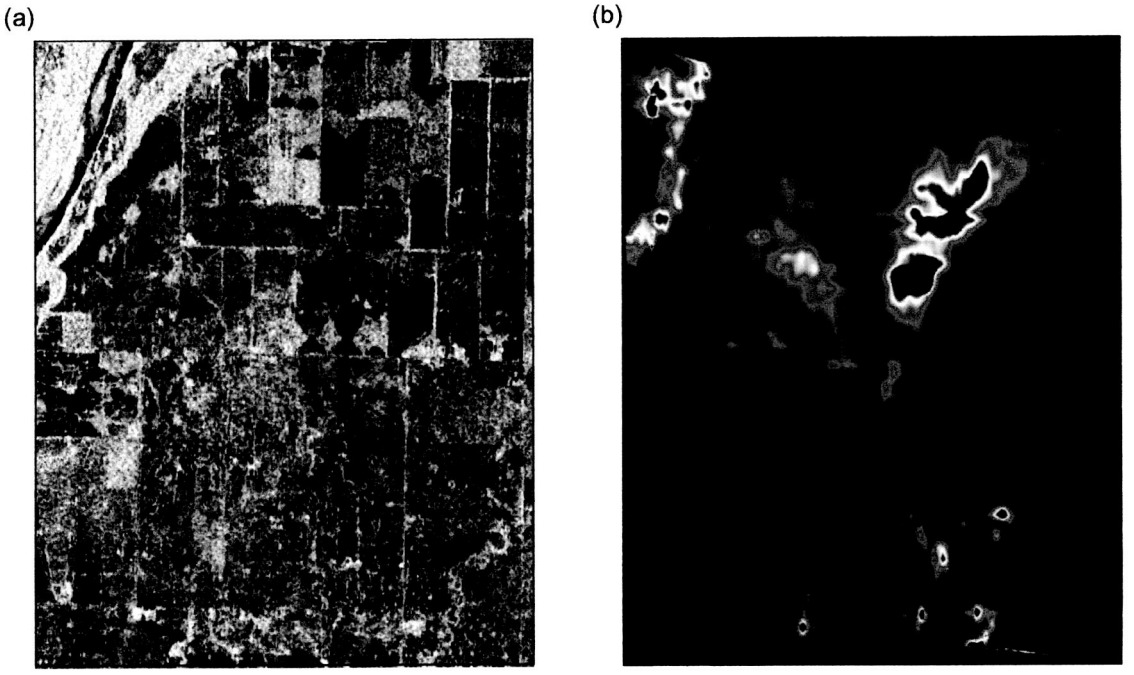


Figure 25. Co-registered images of the Montague Test Site created from (a) radar backscatter for VV polarization (C band = red, L band = green, and P band = blue) and (b) apparent ground conductivity measured at 56,000 Hz. Radar data from AIRSAR flight Montague 180-1.

We quantified the relationship between apparent conductivity and various AIRSAR backscatter modes by (1) choosing a representative airborne EM flight line (line 10210, fig. 20) that crossed the salinity plume and adequately captured the salinization variability within the Montague Test Site, (2) extracted the locations and ungridded apparent conductivity values along that flight line, (3) selected all AIRSAR backscatter values located within 5 m of an apparent conductivity value, and (4) examined the combined conductivity and backscatter data set for spatial correlation and magnitude correlation using individual and combined bands and polarizations. There were 424 apparent conductivity and radar backscatter pairs that fit these criteria along line 10210.

Apparent conductivity measured using the 56,000 Hz airborne induction coils along line 10210 ranged from 30 to 3, 333 mS/m, averaging 519 mS/m (fig. 26). Relatively high conductivities are found over two main lobes of the salinity plume; highest values were measured over the intensely salinized barren area on the Pleistocene terrace of the Red River (figs. 4 and 20).

In the P band, plots of radar backscatter intensity and apparent conductivity with distance along the flight line show little apparent spatial correlation for HH, HV, and VV polarizations alone (fig. 26). Large HH-mode peaks coincide with fence lines; without considering local peaks such as these in each mode, elevated zones of apparent conductivity appear to have little influence on P-band radar backscatter. Radar backscatter intensity range does appear to decrease with increasing apparent conductivity in the HH, HV, and VV modes (fig. 27), which is indicated by weakly negative correlation between backscatter intensity and apparent conductivity in each of the modes (values of –0.14 or less, table 4). The highest range in backscatter intensity is observed for low apparent conductivity values. Backscatter intensity at high apparent conductivity is low in all polarizations.

No apparent spatial correlation exists between conductivity and radar backscatter along line Montague line 10210 for L-band HH, HV, and VV polarizations (fig. 28). Backscatter for each of the polarization modes exhibits decreasing intensity range as conductivity increases (fig. 29), similar to the decrease observed in P-band data. The negative correlation between radar backscat-

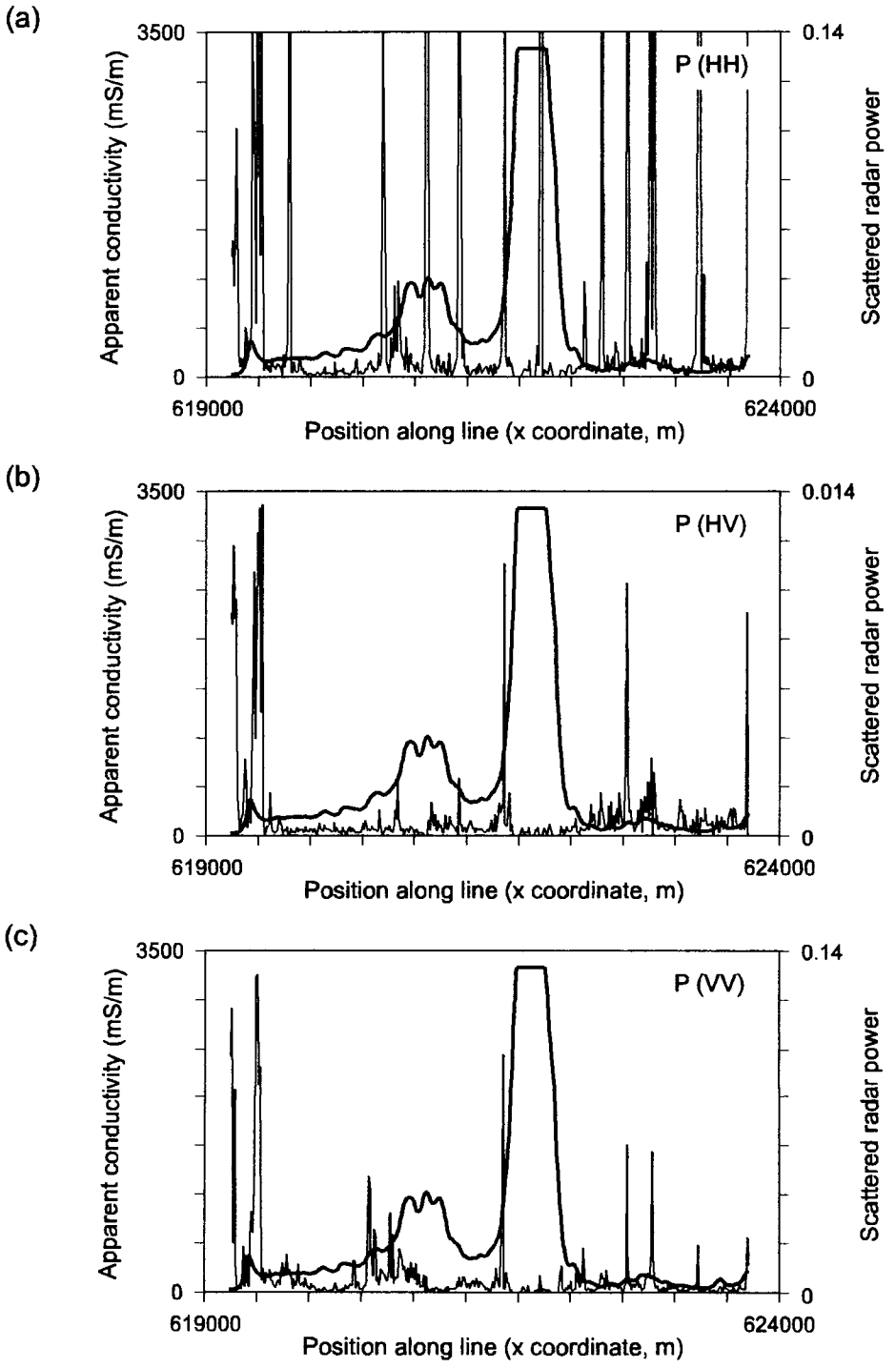


Figure 26. Comparison of P-band backscatter and apparent conductivity measured along Montague flight line 10210 (fig. 20) in the (a) HH, (b) HV, and (c) VV polarizations.

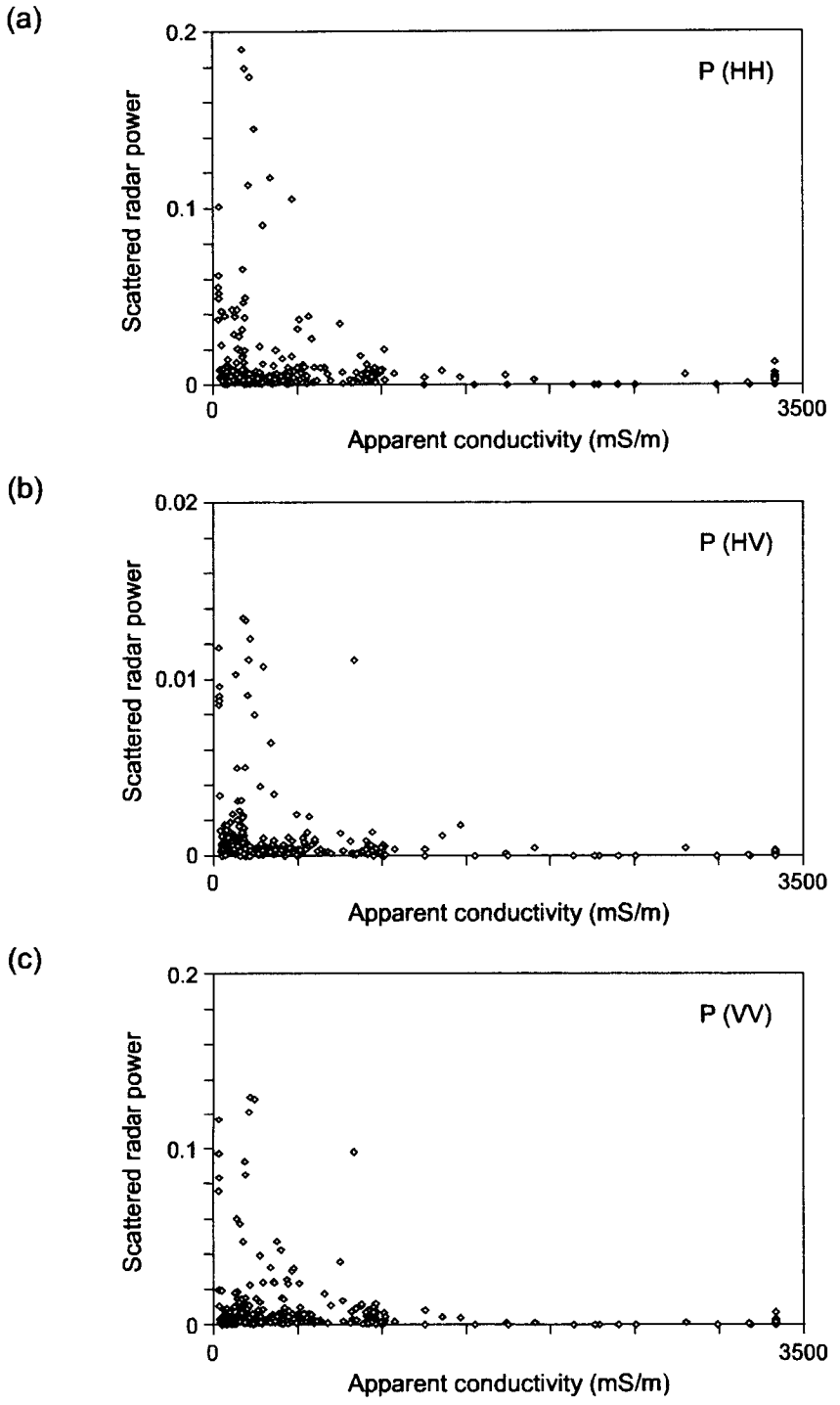


Figure 27. Relationship between apparent conductivity and P-band backscatter in (a) HH, (b) HV, and (c) VV polarizations along Montague flight line 10210.

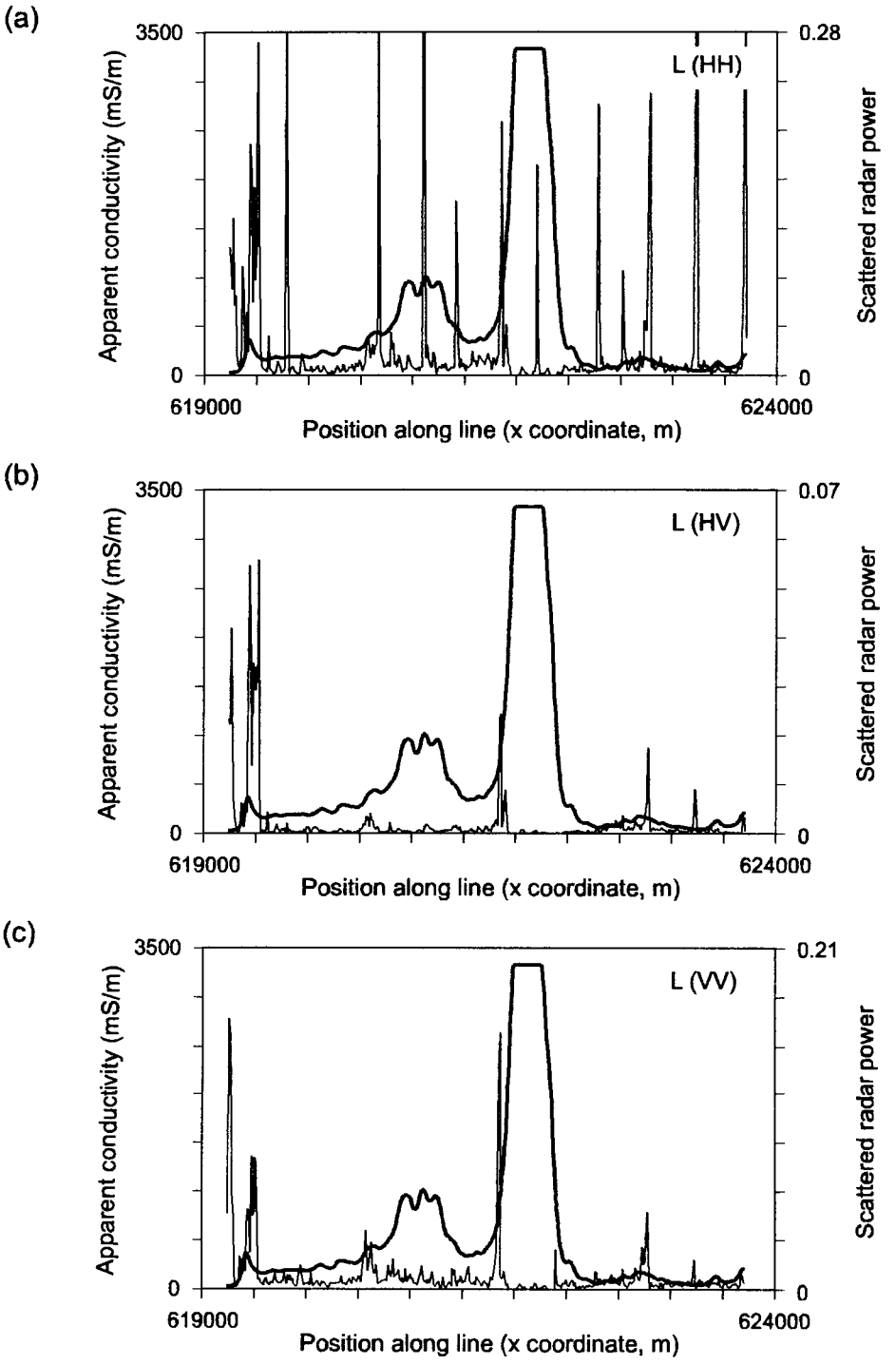


Figure 28. Comparison of L-band backscatter and apparent conductivity measured along Montague flight line 10210 in the (a) HH, (b) HV, and (c) VV polarizations.

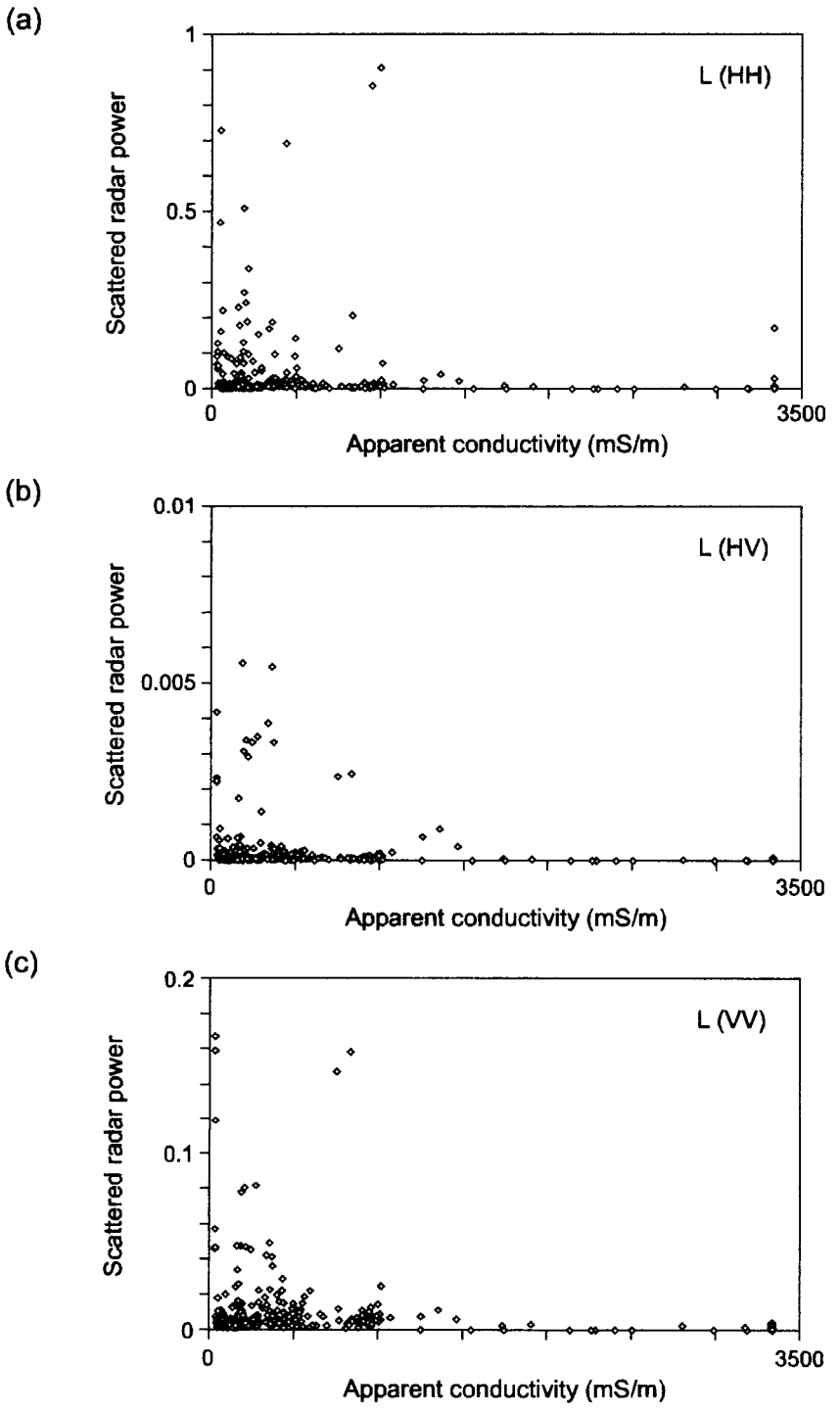


Figure 29. Relationship between apparent conductivity and L-band backscatter in (a) HH, (b) HV, and (c) VV polarizations along Montague flight line 10210.

ter intensity and conductivity is small for L-band data as well, peaking at –0.11 for the VV mode (table 4).

We attempted to enhance the effect of soil electrical properties on radar backscatter by calculating ratios of all combinations of P- and L-band polarizations and examining the spatial and magnitude correlations with measured apparent conductivity. A few radar mode backscatter ratios were relatively highly correlated with apparent conductivity at the Hatchel Test Site (table 4). At the Montague Test Site, all backscatter ratios are poorly correlated with apparent conductivity along line 10210 (fig. 30 and table 4). The three ratios with the highest positive correlation coefficients with apparent conductivity at the Hatchel Test Site (L [VV mode] to L [HV mode], P [VV mode] to L [HV mode], and P [VV mode] to P [HV mode]) all have positive correlation coefficients below 0.1 at the Montague Test Site (fig. 31). Part of the explanation for the poorer correlation at Montague may be that the apparent conductivity values are much higher here than at Hatchel. Power ratio and apparent conductivity appear more positively correlated at conductivities below about 1,500 mS/m, a similar conductivity peak to that observed in the Hatchel area. When we restrict the data pairs used in the correlation coefficient calculation to those with apparent conductivity less than 1,500 mS/m, correlation coefficients improve significantly to 0.25 for L(VV) to L(HV), 0.16 for P(VV) to L(HV), and 0.19 for P(VV) to P(HV). Despite the conductivity range restriction, these values remain lower than those observed from the Hatchel Test Site.

## CONCLUSIONS

High-resolution airborne EM induction surveys of the Hatchel and Montague Test Sites have been shown to accurately map the apparent electrical conductivity of the shallow subsurface. Electrical conductivity of the ground is highly correlated to bulk soil and pore-water salinization, making airborne EM an effective method for identifying salinization and assessing its intensity. The regional applicability of airborne EM is limited because it requires low-flying

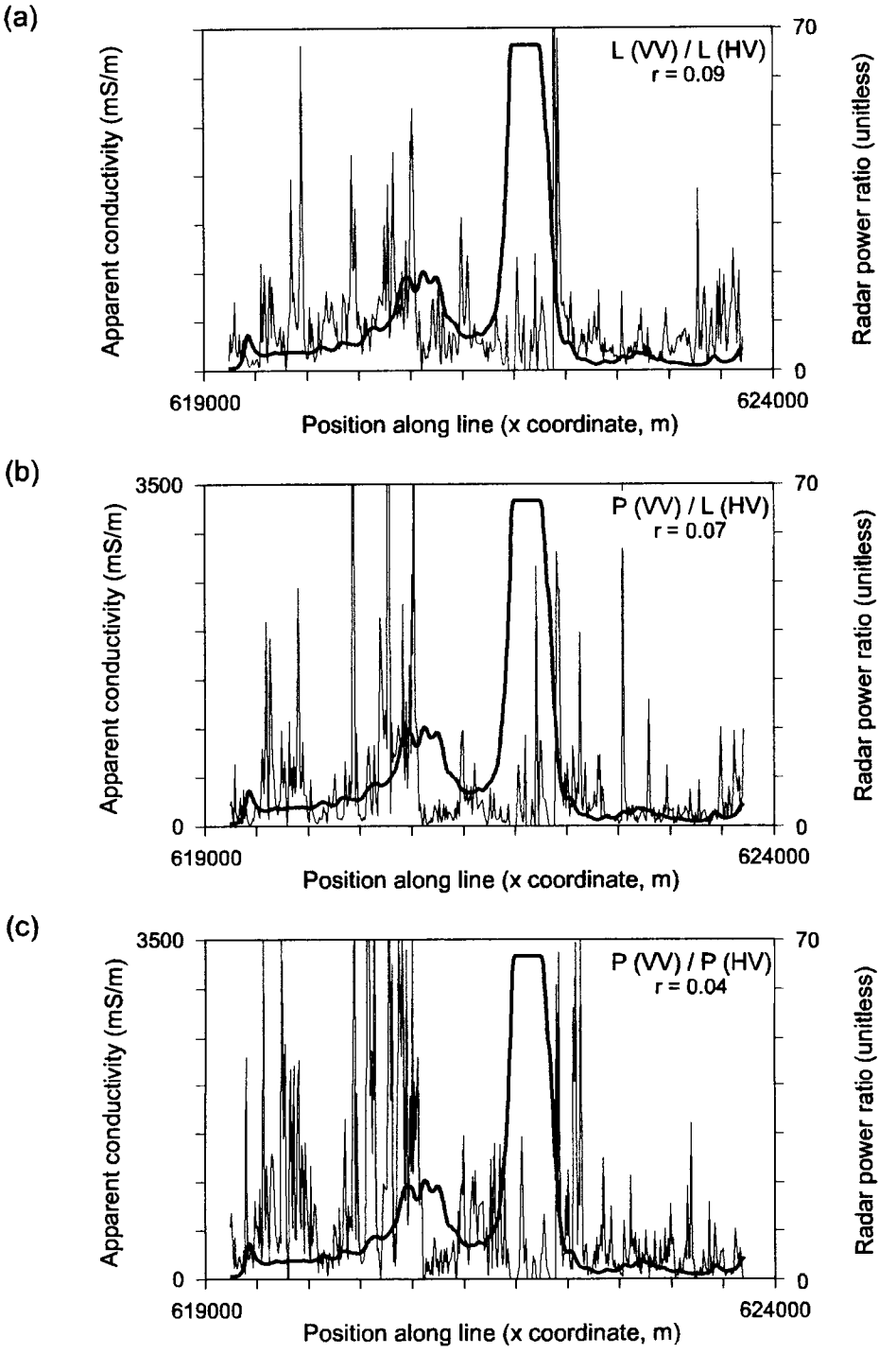


Figure 30. Comparison of radar backscatter ratios and apparent conductivity measured along Montague flight line 10210. The ratios with the three highest correlation coefficients are shown.

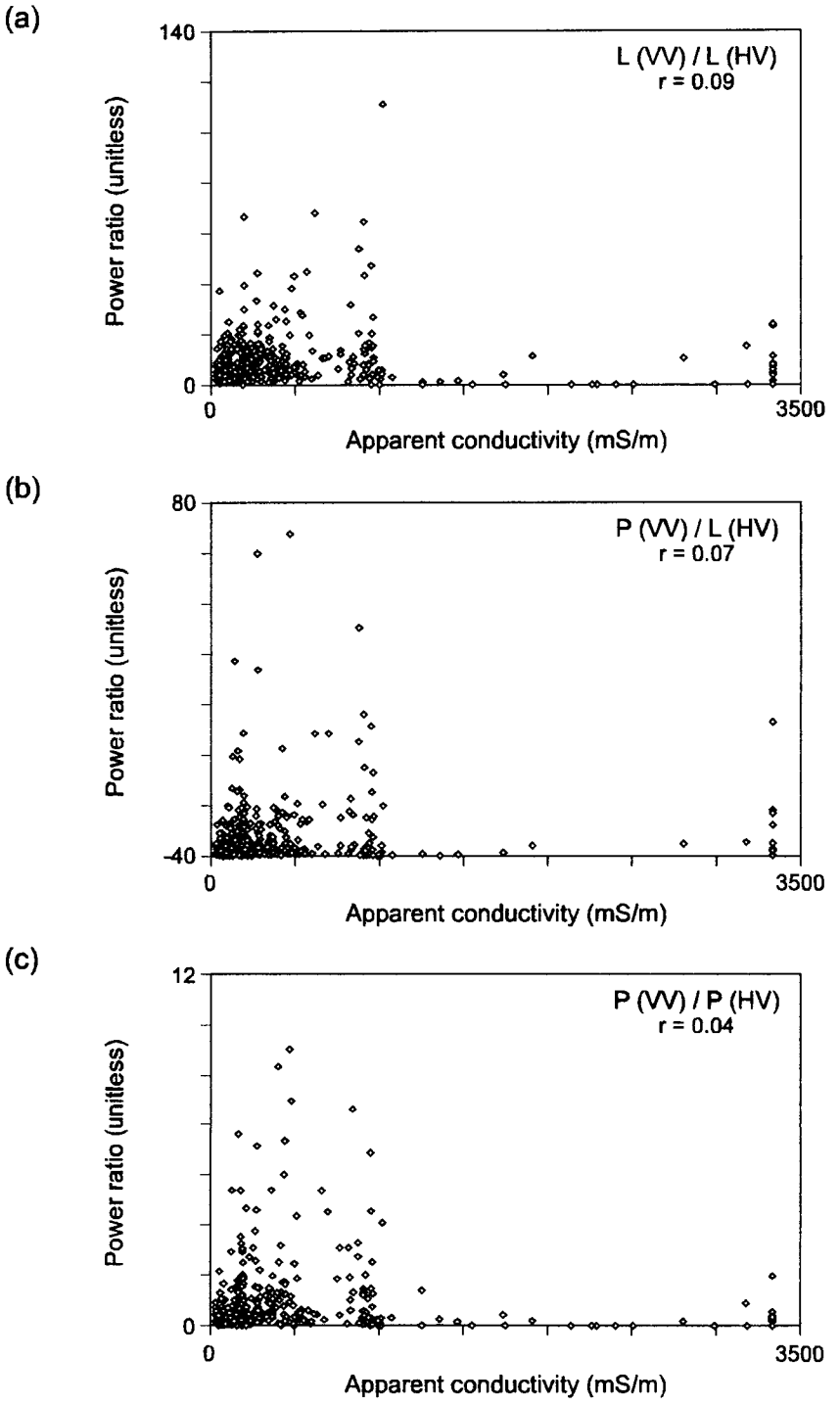


Figure 31. Relationship between apparent conductivity and radar backscatter ratios along Montague flight line 10210. The ratios with the three highest correlation coefficients are shown.

aircraft, making this method prohibitively expensive over broad areas where salinization problems may exist.

Scanning airborne radar data acquired at high altitude using NASA's AIRSAR system can rapidly produce images of relatively large areas at sufficient spatial resolution for salinization screening. No single C-, L-, or P-band polarization correlates well with apparent conductivity measured using airborne EM instruments despite comparisons with the highest available induction frequencies (shallowest exploration depth) at the semiarid Hatchel (West Texas) and Montague (North Texas) Test Sites where both airborne EM and AIRSAR data have been acquired.

A few radar band and polarization ratios appear to enhance the backscattering contribution of shallow soil electrical properties and increase the correlation between conductivity measured at the highest available induction frequency (56,000 Hz) and the radar backscatter ratio. The three radar mode ratios with the highest observed correlation with measured apparent electrical conductivity are L (VV mode) to L (HV mode), P (VV mode) to L (HV mode), and P (VV mode) to P (HV mode). The highest correlation coefficients calculated for radar backscatter ratios and apparent electrical conductivity are higher at the more arid Hatchel Test Site than they are at the wetter Montague Test Site. Correlations at the Montague Test Site improve when data at conductivities higher than those observed at the Hatchel Test Site are excluded from the calculation.

The applicability of airborne radar in salinization mapping appears to be limited by the dominance of vegetation in backscatter response and the limited backscatter return of the oblique radar signal from highly salinized ground with extremely high electrical conductivities. Greater success in soil salinization mapping might be achieved by using an airborne radar system with higher ground incidence angles and a receiving system that records backscatter intensity a few nanoseconds beyond the first backscatter arrival.

## ACKNOWLEDGMENTS

This project was funded by the National Aeronautics and Space Administration under Contract No. NAG5-7582. Herb Frey at the Goddard Space Flight Center served as Technical Officer. Ellen O'Leary at the Jet Propulsion Laboratory oversaw AIRSAR processing. Airborne geophysical data were acquired and processed by Geoterrex-Dighem, now operating as Fugro Airborne Surveys. Bureau of Economic staff Alan Dutton, Martina Blüm, Edward Collins, Susan Hovorka, Jeri Sullivan, Andy Graham, Robin Nava, and Steve Tweedy assisted with supporting geological, geophysical, and hydrological studies.

## REFERENCES

Bomar, G. W., 1983, Texas weather: University of Texas Press, Austin, Texas, 275 p.

Collins, E. W., Paine, J. G., and Raney, J. A., 1999, Summary report for the 1998–1999 STATEMAP project: geological mapping to support improved data-base development and understanding of critical aquifers of Texas: The University of Texas at Austin, Bureau of Economic Geology, report prepared for U.S. Geological Survey, Cooperative Agreement 98HQAG2040, 58 p. + maps.

Frischknecht, F. C., Labson, V. F., Spies, B. R., Anderson, W. L., 1991, Profiling using small sources: in Nabighian, M. N., ed., Electromagnetic methods in applied geophysics—Applications, part A and part B: Tulsa, Oklahoma, Society of Exploration Geophysicists, p. 105–270.

Frye, J. C., and Leonard, A. B., 1963, Pleistocene geology of Red River Basin in Texas: The University of Texas at Austin, Bureau of Economic Geology, Report of Investigations, No. 49, 48 p.

Garrie, D. G., 1996, DIGHEM$^V$ survey for Bureau of Economic Geology, University of Texas, Hatchel study area, Runnels County, Texas: Geoterrex-Dighem, Mississauga, Ontario, Canada, Report 625, not consecutively paginated.

Garrie, D. G., 1997, DIGHEM$^V$ survey for Bureau of Economic Geology, University of Texas, Montague County site, Texas: Geoterrex-Dighem, Mississauga, Ontario, Canada, Report 644, not consecutively paginated.

Hentz, T. F., 1988, Lithostratigraphy and paleoenvironments of upper Paleozoic continental red beds, North-Central Texas: Bowie (new) and Wichita (revised) groups: The University of Texas at Austin, Bureau of Economic Geology, Report of Investigations No. 170, 55 p.

Hovorka, S. D., Dutton, A. R., Paine, J. G., Nava, Robin, and Blüm, M. U., 1999, Site investigation of the Montague salt-water seep, Montague County, Texas: The University of Texas at Austin, Bureau of Economic Geology, contract report prepared for the Railroad Commission of Texas, 133 p.

Kier, R. S., Brown, L. F., Jr., Harwood, P., and Goodson, J. L., 1976, Brownwood sheet: Geologic atlas of Texas: The University of Texas at Austin, Bureau of Economic Geology, Geologic Atlas of Texas, scale 1:250,000.

McBee, W. D., Jr., and Vaughan, L. G., 1956, Oil fields of the central Muenster–Waurika arch: Jefferson County, Oklahoma and Montague County, Texas: in Petroleum geology of southern Oklahoma, Ardmore Geological Society, v. 1, p. 355-372.

McGowen, J. H., Hentz, T. F., Owen, D. E., Pieper, M. K., and Shelby, C. A., 1991, Sherman Sheet (revised from 1967 edition): The University of Texas at Austin, Bureau of Ecomic Geology, Geologic Atlas of Texas, V. E. Barnes, project director, scale 1:250,000.

McNeill, J. D., 1980, Electromagnetic terrain conductivity measurement at low induction numbers: Geonics Ltd., Mississauga, Ont., Technical Note TN-6, 15 pp.

Paine, J. G., 1999, Investigation of geophysical anomalies detected by an airborne survey of the Hatchel area, Runnels County, Texas: The University of Texas at Austin, Bureau of Economic Geology, report prepared for the Railroad Commission of Texas under interagency contract 455-8-8129, 154 p.

Paine, J. G., 2003, Determining salinization extent, identifying salinity sources, and estimating chloride mass using surface, borehole, and airborne electromagnetic induction methods: Water Resources Research, v. 39, no. 3, p. 3-1–3-10.

Paine, J. G., and Collins, E. W., 2003, Applying airborne electromagnetic induction in groundwater salinization and resource studies, West Texas, *in* Proceedings, Symposium on the Application of Geophysics to Engineering and Environmental Problems: Environmental and Engineering Geophysical Society, p. 722–738 (CD-ROM).

Paine, J. G., Dutton, A. R., Blüm, M. U., Boghici, E. M., Nelson, Ianthe, Tremblay, T. A., and Tweedy, S. W., 1997a, Airborne and ground-based geophysical screening of potential brine infiltration sites, Runnels County, Texas: The University of Texas at Austin, Bureau of Economic Geology, final report prepared for Railroad Commission of Texas under Interagency Contract No. 96-0034, 159 p.

Paine, J. G., A. R. Dutton, J. S. Mayorga, and G. P. Saunders, 1997b, Identifying oil-field salinity sources with airborne and ground-based geophysics: a West Texas example: The Leading Edge, v. 16, no. 11, p. 1603-1607.

Paine, J. G., Dutton, A. R., and Blum, M. U., 1999, Using airborne geophysics to identify salinization in West Texas: The University of Texas at Austin, Bureau of Economic Geology, Report of Investigations No. 257, 68 p.

Parasnis, D. S., 1973, Mining geophysics: Elsevier, Amsterdam, 395 p.

Rhoades, J. D., 1981, Predicting bulk soil electrical conductivity versus saturation paste extract electrical conductivity calibrations from soil properties: Soil Science Society of America Journal, v. 45, p. 42-44.

Smith, B. D., Robert Bisdorf, L. J. Slack, and A. T. Mazzella, 1997, Evaluation of electromagnetic mapping methods to delineate subsurface saline waters in the Brookhaven oil field, Mississippi: in Bell, R. S., compiler, Proceedings of the Symposium on the Application of Geophysics to Engineering and Environmental Problems, Env. and Eng. Geophys. Soc., Wheat Ridge, Colo., p. 685-693.

Telford, W. M., L. P. Geldart, R. E. Sheriff, and D. A. Keys, 1976, Applied Geophysics: Cambridge University Press, Cambridge, U.K., 860 pp.

West, G. F., and Macnae, J. C., 1991, Physics of the electromagnetic induction exploration method: in Nabighian, M. N., ed., Electromagnetic methods in applied geophysics—Applications, part A and part B: Tulsa, Oklahoma, Society of Exploration Geophysicists, p. 5-45.

Wiedenfeld, C. C., Barnhill, L. J., Novosad, C. J., 1970, Soil survey of Runnels County, Texas: Soil Conservation Service, U. S. Department of Agriculture, 60 p.